Cell

Article

Custom scoring based on ecological topology of gut microbiota associated with cancer immunotherapy outcome

Graphical abstract

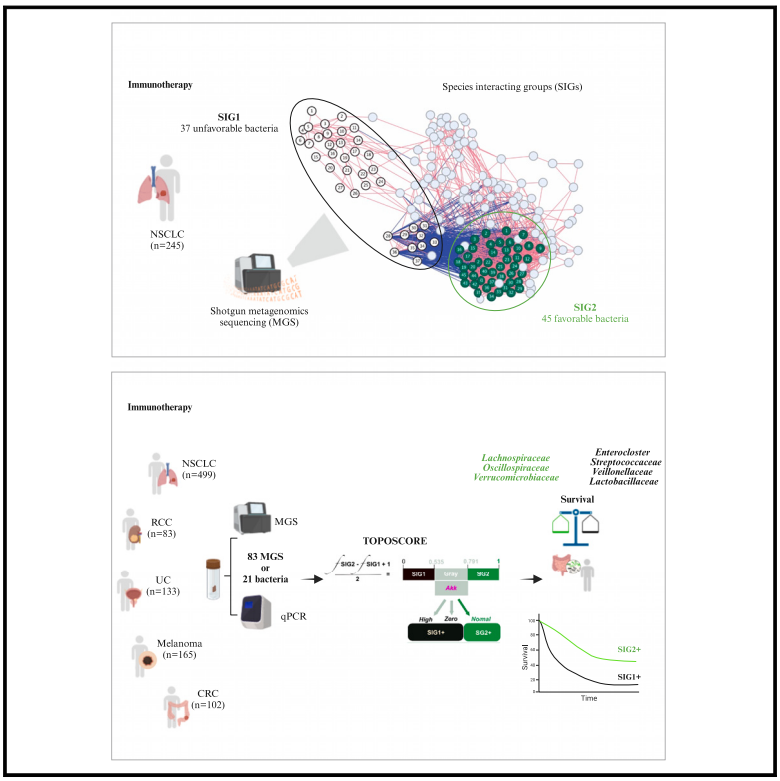

Highlights

- Two topological metagenomic bacterial communities are associated with patient survival
- A unidimensional dysbiosis score was calculated, allowing survival risk stratification
- Gut dysbiosis TOPOSCORE computed from lung cancers could be applied to other cancers
- The metagenomics-based score was translated into a rapid 21-bacteria-based qPCR test

Authors

Lisa Derosa, Valerio Iebba, Carolina Alves Costa Silva, ..., Jérôme Wojcik, Guido Kroemer, Laurence Zitvogel

Correspondence

lisa.derosa@gustaveroussy.fr (L.D.), laurence.zitvogel@gustaveroussy.fr (L.Z.)

In brief

Topological communities of "favorable or unfavorable" bacteria are functional groups in interaction or competition in the gut. The balance between these anti- or pro-inflammatory communities can be translated into a rapid diagnostic test to evaluate the intestinal dysbiosis associated with survival in patients with lung and kidney cancer.

Derosa et al., 2024, Cell *187*, 3373–3389
June 20, 2024
https://doi.org/10.1016/j.cell.2024.05.029

CellPress

Cell

CellPress
OPEN ACCESS

Article

Custom scoring based on ecological topology of gut microbiota associated with cancer immunotherapy outcome

Lisa Derosa,[1,2,3,4,45,46,*] Valerio Iebba,[1,5,45] Carolina Alves Costa Silva,[1,2,3,45] Gianmarco Piccinno,[6] Guojun Wu,[7,8,9] Leonardo Lordello,[1,3] Bertrand Routy,[10,11] Naisi Zhao,[12] Cassandra Thelemaque,[1,3] Roxanne Birebent,[1,2,3] Federica Marmorino,[13,14] Marine Fidelle,[1,2,3] Meriem Messaoudene,[11] Andrew Maltez Thomas,[6] Gerard Zalcman,[15] Sylvie Friard,[16] Julien Mazieres,[17] Clarisse Audigier-Valette,[18] Denis Moro- Sibilot,[19]

(Author list continued on next page)

[1]Gustave Roussy Cancer Campus, ClinicObiome, Villejuif, France
[2]Université Paris-Saclay, Ile-de-France, France
[3]Institut National de la Santé et de la Recherche Médicale (INSERM) U1015, Equipe Labellisée-Ligue Nationale contre le Cancer, Villejuif, France
[4]Department of Medical Oncology, Gustave Roussy, Villejuif, France
[5]Department of Medical, Surgical and Health Sciences, University of Trieste, Trieste, Italy
[6]Department CIBIO, University of Trento, Trento, Italy
[7]Center for Nutrition, Microbiome and Health, New Jersey Institute for Food, Nutrition and Health, Rutgers University, New Brunswick, NJ, USA
[8]Department of Biochemistry and Microbiology, Rutgers University, New Brunswick, NJ, USA
[9]Rutgers-Jiaotong Joint Laboratory for Microbiome and Human Health, New Brunswick, NJ, USA
[10]Centre Hospitalier de l'Université de Montréal (CHUM), Hematology-Oncology Division, Department of Medicine, Montréal, QC, Canada
[11]Centre de Recherche du CHUM (CRCHUM), Montréal, QC, Canada
[12]Department of Public Health and Community Medicine, School of Medicine, Tufts University, Boston, MA 02111, USA
[13]Unit of Medical Oncology 2, University Hospital of Pisa, Pisa, Italy
[14]Department of Translational Research and New Technologies in Medicine and Surgery, University of Pisa, Pisa, Italy
[15]Université Paris Cité, Thoracic Oncology Department-CIC1425/CLIP2 Paris-Nord, Bichat-Claude Bernard Hospital, AP-HP, Paris, France
[16]Pneumology Department, Foch Hospital, Suresnes, France
[17]Centre Hospitalier Universitaire de Toulouse, Toulouse, France
[18]Pneumology Department, Centre Hospitalier Toulon Sainte-Musse, Toulon, France
[19]Department of Thoracic Oncology, Centre Hospitalier Universitaire, Grenoble, France

(Affiliations continued on next page)

SUMMARY

The gut microbiota influences the clinical responses of cancer patients to immunecheckpoint inhibitors (ICIs). However, there is no consensus definition of detrimental dysbiosis. Based on metagenomics (MG) sequencing of 245 non-small cell lung cancer (NSCLC) patient feces, we constructed species-level co-abundance networks that were clustered into species-interacting groups (SIGs) correlating with overall survival. Thirty-seven and forty-five MG species (MGSs) were associated with resistance (SIG1) and response (SIG2) to ICIs, respectively. When combined with the quantification of *Akkermansia* species, this procedure allowed a person-based calculation of a topological score (TOPOSCORE) that was validated in an additional 254 NSCLC patients and in 216 genitourinary cancer patients. Finally, this TOPOSCORE was translated into a 21-bacterial probe set-based qPCR scoring that was validated in a prospective cohort of NSCLC patients as well as in colorectal and melanoma patients. This approach could represent a dynamic diagnosis tool for intestinal dysbiosis to guide personalized microbiota-centered interventions.

INTRODUCTION

Microbial symbionts inhabiting our mucosae play crucial roles in biogeochemical cycles and human health.[1] The biological properties of microbial communities are determined by their taxonomic composition. Shifts in the gut microbiome, for instance, have been directly linked to multiple chronic inflammatory disorders, including cancer.[2,3] Tumorigenesis can induce a stress ileopathy that promotes a protracted intestinal dysbiosis, often characterized by the relative overrepresentation of the

François Goldwasser,[20,21,22] Arnaud Scherpereel,[23] Hervé Pegliasco,[24] François Ghiringhelli,[25,26,27] Nicole Bouchard,[28] Cissé Sow,[1,3] Ines Darik,[1,3] Silvia Zoppi,[1,3,29] Pierre Ly,[1,3] Anna Reni,[1,3,30] Romain Daillère,[31] Eric Deutsch,[1,2,32,33] Karla A. Lee,[34] Laura A. Bolte,[35] Johannes R. Björk,[35] Rinse K. Weersma,[35] Fabrice Barlesi,[1,2,4] Lucas Padilha,[36] Ana Finzel,[36] Morten L. Isaksen,[36] Bernard Escudier,[1,4] Laurence Albiges,[1,2,4] David Planchard,[1,2,4] Fabrice André,[1,2,4] Chiara Cremolini,[13,14] Stéphanie Martinez,[37] Benjamin Besse,[1,2,4] Liping Zhao,[7,8,9,38] Nicola Segata,[6,39] Jérôme Wojcik,[40] Guido Kroemer,[1,41,42,43] and Laurence Zitvogel[1,2,3,44,*]

[20]INSERM U1016-CNRS UMR8104, Paris Cité University, Paris, France
[21]Department of Medical Oncology, Cochin Hospital, Assistance Publique-Hôpitaux de Paris, Paris, France
[22]Immunomodulatory Therapies Multidisciplinary Study Group (CERTIM), Paris, France
[23]Department of Pulmonary and Thoracic Oncology, University of Lille, University Hospital (CHU), Lille, France
[24]Pulmonary Department, European Hospital, Marseille, France
[25]Cancer Biology Transfer Platform, Centre Georges-François Leclerc, Dijon, France
[26]Centre de Recherche INSERM LNC-UMR1231, Dijon, France
[27]Department of Medical Oncology, Centre Georges-François Leclerc, Dijon, France
[28]Centre Hospitalier de Sherbrooke, Sherbrooke, QC, Canada
[29]Department of Medicine and Surgery, University of Parma, Parma, Italy
[30]Section of Oncology, Department of Medicine, University of Verona School of Medicine and Verona University Hospital Trust, Verona, Italy
[31]EverImmune, Gustave Roussy Cancer Campus, Villejuif, France
[32]Department of Radiation Oncology, Gustave Roussy, Villejuif, France
[33]INSERM U1030, Radiothérapie Moléculaire et Innovation Thérapeutique, Villejuif, France
[34]Department of Twin Research and Genetic Epidemiology, King's College London, London, UK
[35]Department of Gastroenterology and Hepatology, University of Groningen and University Medical Center Groningen, Groningen, the Netherlands
[36]Bio-Me AS, Oslo Science Park, Gaustadalléen 21, Oslo, Norway
[37]Service des Maladies Respiratoires, Centre Hospitalier d'Aix-en-Provence, Aix-en-Provence, France
[38]State Key Laboratory of Microbial Metabolism, Ministry of Education Laboratory of Systems Biomedicine, Shanghai Jiao Tong University, Shanghai, China
[39]IEO, European Institute of Oncology IRCCS, Milan, Italy
[40]Data2time Sàrl, Froideville, Switzerland
[41]Centre de Recherche des Cordeliers, Equipe labellisée—Ligue contre le cancer, Université de Paris Cité, Sorbonne Université, Institut Universitaire de France, Inserm U1138, Paris, France
[42]Metabolomics and Cell Biology Platforms, Gustave Roussy, Villejuif, France
[43]Institut du Cancer Paris CARPEM, Department of Biology, Hôpital Européen Georges Pompidou, Assistance Publique-Hôpitaux de Paris, Paris, France
[44]Center of Clinical Investigations in Biotherapies of Cancer (BIOTHERIS) 1428, Villejuif, France
[45]These authors contributed equally
[46]Lead contact
*Correspondence: lisa.derosa@gustaveroussy.fr (L.D.), laurence.zitvogel@gustaveroussy.fr (L.Z.)
https://doi.org/10.1016/j.cell.2024.05.029

immunosuppressive *Enterocloster* genus that induces resistance to PD-1 blockade.[4] However, fecal microbial transplantation (FMT) may circumvent primary resistance to immunotherapy in melanoma by inducing distinct ecological changes accompanied by anti-inflammatory, immunological, and metabolic reprogramming of the original microbiota and tumor microenvironment of the recipient.[5,6] Indeed, clinical benefit to immune-checkpoint inhibitors (ICIs) or chimeric antigen receptor-T cell therapy has been linked to the presence or absence of distinct intestinal commensals across various malignancies.[7–11] Of note, antibiotics (except vancomycin),[4,12] proton pump inhibitors,[13,14] and probiotics may alter the taxonomic composition of the intestinal microbiota, resulting in resistance to immunotherapy.[15–17]

Beneficial gut ecosystems, comprising, among others, several *Lachnospiraceae* and *Ruminococcaceae* family members, as well as species from *Faecalibacterium*, *Akkermansia*, and *Bifidobacterium* genera, harbor pattern recognition receptor ligands, produce metabolites (such as short-chain fatty acids, L-arginine, inosine, or tryptophan), and express cancer antigen mimetics that can elicit type 1 interferon (IFN) or interleukin-12 (IL12)-mediated TH1 or follicular T helper cell responses during immunotherapy.[18–21] Despite compelling evidence for beneficial and harmful metagenomic species (MGSs) associated with clinical outcome in at least 18 ancillary studies,[22,23] little consensus exists on which microbiome signatures are commonly associated with treatment responses.[24–26] Additionally, there is a need for user-friendly tools to support the application of microbiome profiling of clinically significant intestinal dysbiosis in routine oncology practice.

Several confounding factors may have contributed to this lack of consensus, such as technical considerations (fecal sample collection methods and DNA extraction protocols), geographical differences in patient populations (different diets and medications across different countries), statistical reasons (such as inter-patient variability, small sample size), different definitions of treatment outcomes (e.g., grouping stable disease with non-responders [NR] or responders [R], or using progression-free survival [PFS] instead of best clinical response as outcome measure), and the significance of microbial signals that are functionally related but driven by different species.[26] Although interest in defining the commensal gut microbiome has grown,

our understanding of microbial interactions within communities is still limited. Moreover, it remains difficult to predict which groups of microbes would form a stable community and how a given community would respond to intrinsic (pathological) or external (therapeutic) perturbations. In addition, although resource competition, metabolic cross-feeding, and niche availability are among the main drivers of microbial community assembly,[27–29] the effect of host comorbidities and comedications on the gut microbiome is still being elucidated. Co-abundance network analysis to identify "guilds," or functional groups consisting of diverse but cooperative bacteria, seems to be a promising approach for identifying microbial sub-communities as units relevant to host metabolic health or disease progression.[27,30]

Based on shotgun metagenomics (MG) sequencing of fecal materials at baseline, we constructed a co-abundance network depicting relative abundance interrelationships within a discovery cohort of 245 patients with advanced non-small cell lung cancer (NSCLC). This network identified several microbial sub-consortia, or sub-communities, named "species-interacting groups" (SIGs), leading to the identification of two main SIGs driving the clinical response to PD-1 blockade in advanced NSCLC, namely, "SIG1" comprising 37 bacteria associated with poor responses and "SIG2" encompassing 45 bacteria associated with good responses. The calculation of the SIG1/SIG2 ratio for each individual mirrored the seesaw balance between these interactive groups. Individuals with a score falling into an intermediate category ("gray zone," neither SIG1 nor SIG2) could be further segregated based on the relative abundance of *Akkermansia spp.*, as previously described.[31] The combination of the SIG1/SIG2 ratio and *Akkermansia muciniphila* (*Akk*) abundance yielded a topological score (TOPOSCORE) estimating the likelihood of an individual to respond to PD1/PD-L1 blockade in a second cohort of 254 NSCLC patients (in 1st or 2nd line (L) therapy) and a third cohort of 216 kidney renal cell cancer (RCC) and urothelial cancer (UC) patients. Using the TOPOSCORE, we observed that 20%, 53%, 58%, 35%, and 57% of healthy volunteers, 1st L NSCLC, 2nd L NSCLC, 2nd L RCC, and 2nd L UC, respectively, presented with gut dysbiosis. We finally scaled down the calculation of the TOPOSCORE to 21 MGSs and set up a qPCR-based user-friendly test capable of accurately identifying the fecal presence of the selected 21 bacteria. The reduced 21 MGS-based TOPOSCORE was associated with immunotherapy outcome in melanoma and colorectal cancer patients. By converting the TOPOSCORE to a qPCR-based test with a 48 h turnaround time, it will be possible to adopt this score in routine clinical practice to improve patient stratification. Moreover, the observational cohorts encompassing a total of 872 NSCLC, genitourinary, and colorectal cancer patients reported here provide a resource for correlating ICI responses with the gut microbiota.

RESULTS

Limitations in predicting clinical outcome across cohorts and cancer types using single MGS

LUMIERE and ONCOBIOTICS are two prospective observational studies (NCT03084471) recruiting 499 patients with advanced NSCLC in France and Canada since 2017 as well as 83 patients with RCC in France. For each patient, stool samples were available before and during treatment (within 1 and 3 months of treatment start) and could be matched with detailed clinical data, including information relative to comedications (Table S1). To study the prognostic impact of the gut microbiota composition on ICI responses in NSCLC and RCC, we performed MG sequencing of frozen fecal samples in a partially reported[7,9] discovery cohort (enrolling NSCLC patients from 2017 to 2019, n = 245) and in a partially reported[31] validation cohort (enrolling NSCLC patients from 2019 to 2023, n = 254) (Table S1).

We first determined whether the fecal taxonomic composition at baseline (at the species level as previously reported[7,9,31]) in the discovery cohort composed of 245 NSCLC patients would be associated with overall survival (OS) beyond 12 months (OS $\geq$ 12) upon 1st L or $\geq$2nd L therapy with anti-PD-1 or anti-PD-L1 antibodies (Abs). From the MG of the discovery cohort, 536 MGSs were identified using MetaPhlAn 4.0. To characterize differences in microbial composition between patient groups achieving OS < 12 (NR, n = 112) or OS $\geq$ 12 (R, n = 118), we monitored the differences in stool microbial alpha diversity and performed principal coordinate analyses (PCoA) of microbial beta-diversity distances (Bray-Curtis on normalized and standardized data as described in the STAR Methods session). Of note, 15 patients did not reach a 12-month-minimal follow up and could not be included in this analysis. Alpha diversity (as defined as Shannon index, inverse Simpson, or number of observed taxa) was significantly different in the two groups with a higher richness in R (Figure S1A). Next, we utilized an unsupervised PCoA to explore putative differences in general microbiota composition between short- and long-term survivors by means of two metrics, i.e., analysis of similarities (ANOSIM) and permutational multivariate analysis of variance (PERMANOVA) computed on the Bray-Curtis distance matrix. Both metrics revealed a difference between the two groups (ANOSIM R = 0.031, p = 0.0039; PERMANOVA F = 2.895, p = 0.0029) (Figure S1A). To determine the relative contribution of each microbial species abundance at baseline to the observed group separation, MGSs were ordered according to their variable importance (VIP) score (Figure S1A), which relies on the supervised partial least squares discriminant analysis (PLS-DA). Some of the MGSs that were significantly associated with OS < 12 were already described in antibiotic-treated or poor prognosis cancer patients (such as *Hungatella hathewayi*, *Clostridium innocuum*, *Streptococcus anginosus*, or *Actinomyces graevenitzii*).[9,32]

Next, we analyzed the validation NSCLC cohort (enrolled until 2022) in which slightly more therapy-naive patients were enrolled than in the discovery cohort (Table S1). Alpha diversity (Figure S1B, p = 0.4413) was not different between OS < 12 and OS $\geq$ 12 subsets. The beta-diversity (Figure S1B, ANOSIM R = 0.017, p = 0.0489; PERMANOVA F = 2.123, p = 0.0297) was able to segregate the two groups. Considering strictly MGSs identified using the MetaPhlAn 4.0 pipeline commonly found in both cohorts (discovery and validation), we only recovered four shared MGSs associated with OS $\geq$ 12, including *Anaerostipes hadrus* (Figures S1A and S1B). The Cox regression analysis of OS based on the prevalence (presence or absence) of *A. hadrus* was significantly associated with long-term clinical benefit to PD-1 blockade, in both the discovery and the

1. *Actinomyces graevenitzii*	29. *Enterocloster aldensis*	4. *Megasphaera micronuciformis*
6. *Alloscardovia omnicolens*	35. *Enterocloster bolteae*	14. *Streptococcus anginosus*
37. *Anaerostipes caccae*	32. *Enterocloster clostridioformis*	27. *Proteus mirabilis*
33. *Blautia producta*	28. *Erysipelatoclostridium ramosum*	10. *Streptococcus gordonii*
13. *Bifidobacterium dentium*	24. *Fournierella massiliensis*	9. *Streptococcus mutans*
7. *Campylobacter concisus*	17. *Granulicatella adiacens*	22. *Streptococcus oralis*
21. *Campylobacter gracilis*	30. *Hungatella hathewayi*	8. *Streptococcus parasanguinis*
36. *Clostridium innocuum*	25. *Lacticaseibacillus paracasei*	2. *Streptococcus salivarius*
12. *Clostridium perfringens*	26. *Lactobacillus gasseri*	5. *Veillonella atypica*
31. *Clostridium scindens*	15. *Lactobacillus vaginalis*	3. *Veillonella dispar*
34. *Clostridium symbiosum*	16. *Ligilactobacillus salivarius*	11. *Veillonella parvula*
23. *Collinsella SGB14754*	19. *Limosilactobacillus fermentum*	
18. *Enorma massiliensis*	20. *Limosilactobacillus oris*	

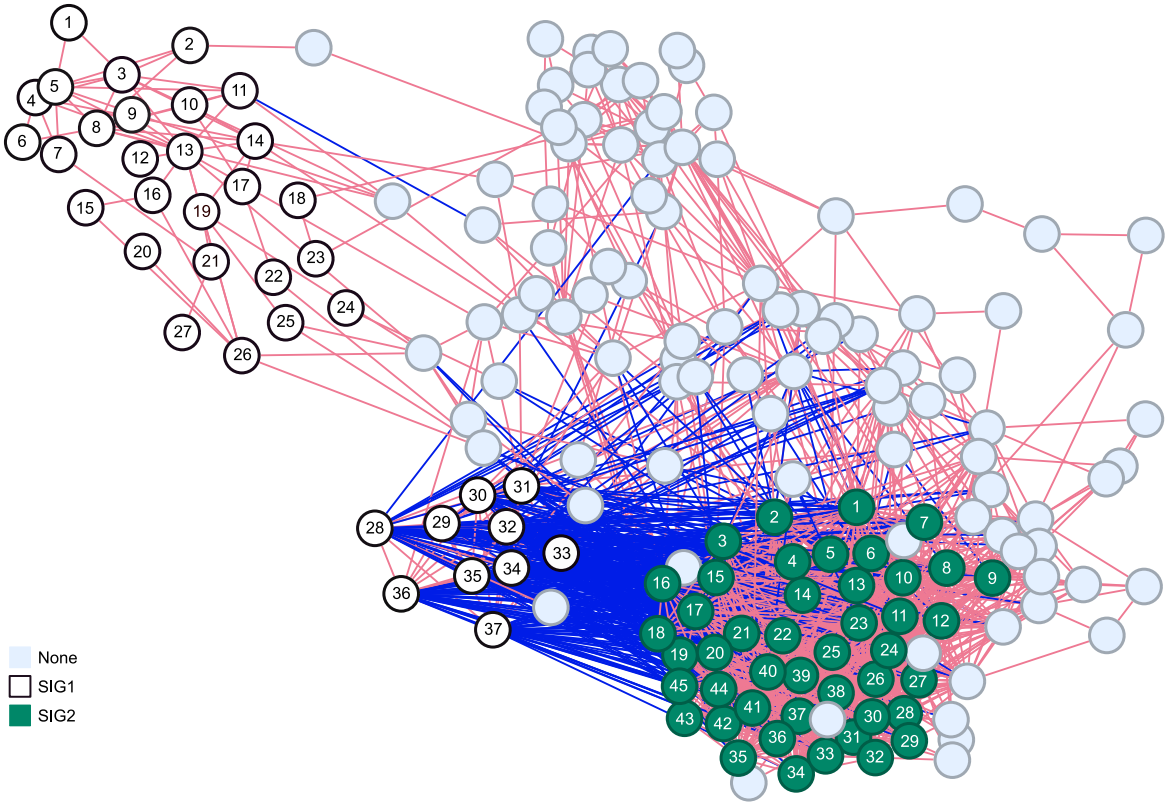

37. *Agathobaculum butyriciproducens*	13. *Clostridium sp AM33 3*	38. *Lachnospira eligens*
19. *Anaerobutyricum hallii*	44. *Clostridium sp AM49 4BH*	45. *Lachnospira pectinoschiza*
42. *Anaerostipes hadrus*	4. *Coprobacter fastidiosus*	3. *Lachnospira sp NSJ 43*
28. *Anaerotignum faecicola*	6. *Coprococcus comes*	7. *Lachnospiraceae bacterium OM04 12BH*
31. *Blautia massiliensis*	2. *Coprococcus eutactus*	10. *Lachnospiraceae bacterium WCA3 601 WT 6H*
34. *Blautia wexlerae*	14. *Dorea formicigenerans*	17. *Lacrimispora amygdalina*
5. *Candidatus Cibiobacter qucibialis*	22. *Dorea longicatena*	24. *Mediterraneibacter butyricigenes*
43. *Clostridiaceae bacterium*	29. *Eubacterium ramulus*	11. *Oscillibacter sp ER4*
25. *Clostridiaceae bacterium OM08 6BH*	33. *Eubacterium rectale*	9. *Phocaeicola massiliensis*
8. *Clostridiaceae unclassified SGB4769*	30. *Eubacterium ventriosum*	41. *Roseburia hominis*
21. *Clostridiales bacterium KLE1615*	15. *Faecalibacillus intestinalis*	35. *Roseburia intestinalis*
12. *Clostridiales unclassified SGB15145*	39. *Faecalibacterium prausnitzii*	36. *Roseburia inulinivorans*
27. *Clostridium fessum*	1. *Faecalibacterium SGB15346*	32. *Roseburia sp AF02 12*
20. *Clostridium sp AF34 10BH*	40. *Firmicutes bacterium AF16 15*	16. *Ruminococcus bicirculans*
26. *Clostridium sp AM22 11AC*	23. *Gemmiger formicilis*	18. *Ruminococcus lactaris*

(legend on next page)

validation cohorts (Figures S1C and S1D). Despite these apparently encouraging results, the StratifiedKFold (*n*_splits = 5) random forest (RF) receiver operating characteristic (ROC) curves,[33] measuring the performance of the relative abundance of these MGSs to classify patients into OS < 12 or ≥ 12, indicated area under the ROC curve (AUC) values around 0.6 in the whole NSCLC cohort (discovery + validation, *n* = 499), suggesting that these microbial species, alone or in a 4-species cumulative RF model, were not able to robustly dictate patients' treatment responses (Figures S1E–S1G). Moreover, in the context of another malignant disease, in a cohort of RCC patients, the prevalence of *Anaerostipes hadrus* spp failed to predict long-term survival (Figure S1H). In fact, *A. hadrus* spp correspond to highly prevalent (around 70%) (Figures S1C and S1D, right panels) and relatively abundant species, suggesting that they are necessary but not sufficient to accurately select patients with better prognosis. Hence, as previously discussed,[26] despite large and homogeneous cohorts handled by the same investigators using a clinically relevant endpoint (OS at 12 months, OS12), we failed to identify a prototypical MGS fingerprint robustly predicting clinical benefit to PD-1 blockade across several malignancies.

Co-abundance networks within the microbial ecosystem of NSCLC patients

The ecosystem community structural organization and the degree to which such forces interact in long-term R or NR have not been investigated to date. Here we used prevalence and/or relative abundances of MGSs to assess their cooperative potential within large SIGs and the clinical relevance of SIGs for the response to PD-1 blockade in the discovery cohort.

Building intestinal communities (SIGs)

Each MGS was categorized as either "low" or "high" based on the median of its relative abundance in the whole population of 245 subjects (≤ median or > median, respectively). For those MGSs that had a majority of null abundances (i.e., median = 0), the MGSs were categorized as "present" or "absent" (relative abundance > 0 or = 0, respectively). Cox proportional-hazard (CoxPH) models were run to select MGSs associated with an elevated or reduced OS with a hazard ratio (HR) ≤ 0.80 or ≥ 1.25, respectively. The purpose of this selection was to discard MGSs with HR close to 1, which are unlikely to contribute to the robustness of the signature. Among the 536 MGSs identified in the discovery cohort, a total of 266 MGSs were retained in the model (Table S2A). The Akk MGSs (as well as *Alistipes senegalensis* and *Bacteroides caccae*) were not considered in this screening because their functional impact on NSCLC prognosis was trichotomic (or not significant for the two others) with no linear dose-effect relationship with patient prognosis.[31] Each pair of these 266 MGSs was then analyzed by Fisher's exact test on 2 × 2 contingency tables based on their absence/presence co-occurrences and scored by the $-log_{10}(p) \times sign(OR - 1)$ metrics, where p is the Fisher p value and OR, the odds ratio of the 2 × 2 table. This metric defined a score proportional to the significance of the interaction between two MGSs ($-log_{10}(p)$) that is negative in case of co-exclusion pattern (OR < 1) or positive in case of co-occurrence (OR > 1). Interactions with a Bonferroni-corrected p value ≤ 0.05 were retained for analysis (Figure S2A). A total of 180 connected MGSs were then clustered with Ward's method and Manhattan distance, resulting in the identification of 7 clusters (C1 to C7) (Figures S3A and S3B; Table S2A). Two clusters (C5 and C6) contained 37 MGSs, mostly (95%) associated with OS < 12 (HR ≥ 1.25) that were used to define the SIG1 signature. Three clusters (C1, C2, and C3) that contained 45 MGSs all associated with OS > 12 months (HR ≤ 0.80) were compounded into the SIG2 signature (Figure S3A; Table S2B). All the other clusters failed to correlate with OS. In addition, interactions within SIG1 and SIG2 MGSs were ≥99% positive (indicating close-to-perfect co-occurrence patterns), while edges in-between SIG1 and SIG2 MGSs were 98% negative (indicating a significant co-exclusion pattern), thus reflecting a sharp and reproducible topological separation (Figure 1A). This interpretation is supported by the fact that SIG1 contained members belonging to the *Enterocloster* genus and *Streptococcaceae*, *Veillonellaceae*, and *Lactobacillaceae* families that were already associated with dismal prognosis and immunoresistance.[4,17,25,26,32] Conversely, SIG2 contained *Lachnospiraceae* (species from the genus *Blautia*, *Roseburia*, *Dorea*, and *Eubacterium*) and *Oscillospiraceae* family members (*Faecalibacterium prausnitzii, Ruminococcus bicirculans*, and *R. lactaris*), which were previously associated with general health and favorable clinical responses to ICIs.[8,34]

Scoring system for each individual

Next, we reduced the information on this whole-population-based network to a unidimensional score. Each patient of the discovery cohort received an S score computed as the difference of proportions between present (relative abundance > 0) SIG2 and SIG1 MGSs and scaled from 0 to 1: $S = (\#SIG2/45 - \#SIG1/37 + 1)/2$. A score of 0 would indicate that all MGSs of the SIG1 signature but none of the SIG2 signature are detectable. Conversely, a score of 1 would indicate that all MGSs of the SIG1 are undetectable, contrasting with the detection of all MGSs of the SIG2 signature. For MGSs with various annotated species at the species-level genome bins (SGB) level of resolution in *MetaPhlAn4* (such as *Faecalibacterium prausnitzii* identified as SGB15316, SGB15318, SGB15322, SGB15323, SGB15332, and SGB15342), we considered the prevalence of at least one of these subspecies for each patient. The performance of this S score as predictor of OS12 was analyzed by a ROC analysis. Two scores, 0.5351 and 0.7911, were identified as local maxima of the Youden index (specificity + specificity − 1, Figure S2B) and were used as cutoff values to define three categories: SIG1 if $S \leq 0.5351$, SIG2 if $S \geq 0.7911$, and otherwise a gray

Figure 1. Co-abundance networks and species-interacting groups (SIGs) associated with response or resistance to ICIs in the discovery cohort of NSCLC

Microbial network of the discovery cohort (*n* = 245) using co-occurrence matrices of 180 selected MGSs. Edges are significant ($p \leq 0.001$) Fisher associations (pink and blue lines for co-occurrence and co-exclusion patterns, respectively). Nodes (representing MGSs) were colored according to SIG1 (black) or SIG2 (green), while others were left in light blue circled in gray. See also Figures S2 and S3. Numbers in the circles correspond to MGSs identification whose specific taxonomic nomenclatures are aligned in the upper (SIG1) or lower parts (SIG2) of the graph.

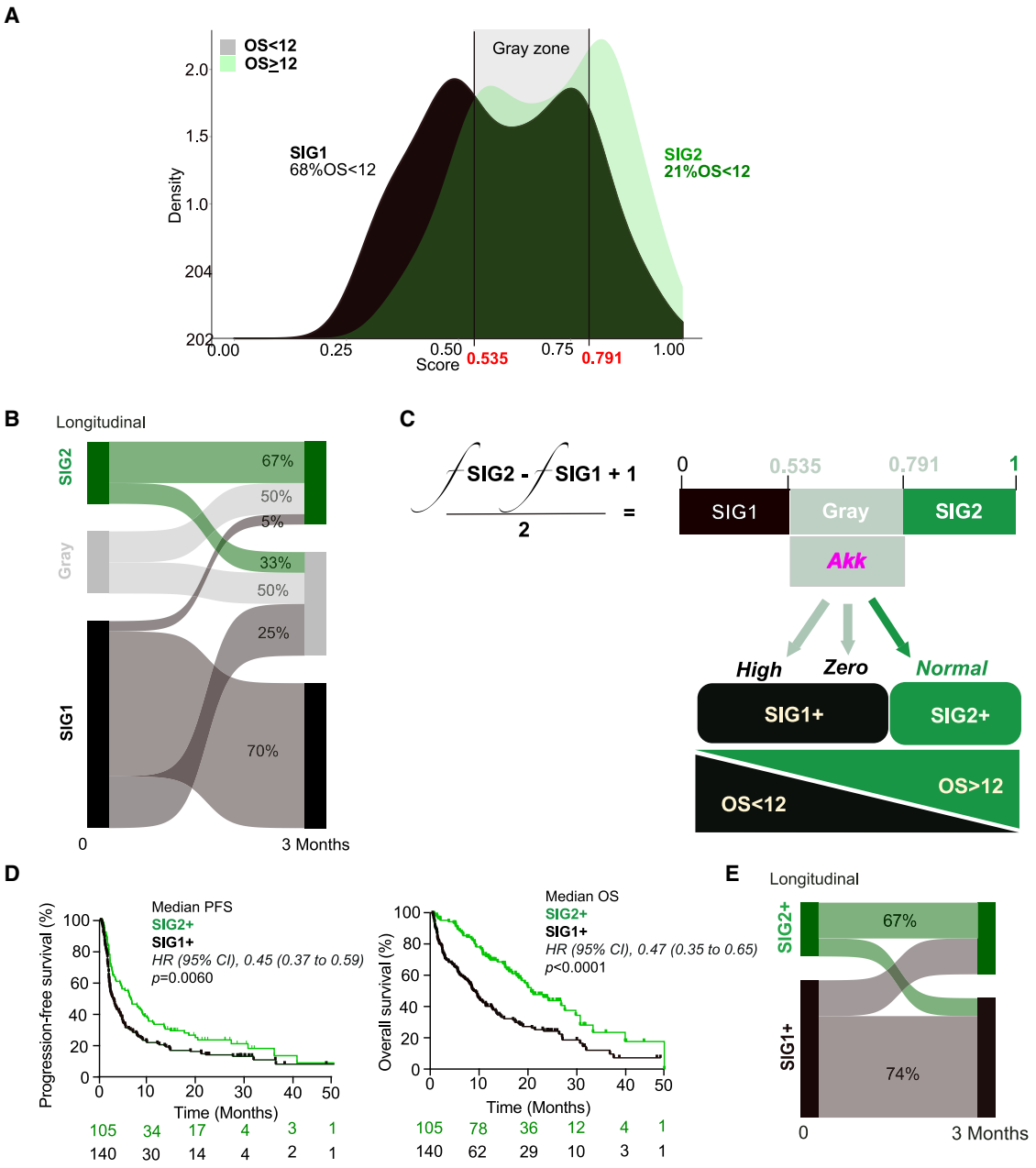

Figure 2. Design and performance of the TOPOSCORE in the discovery cohort

(A) The distribution of the S score is depicted by means of kernel density estimation (KDE). The boundaries between these two SIG distributions—identified as local maxima of the Youden index (0.5351 and 0.7911)—are indicated in the x axis and individualize the limits of the gray zone. The percentages of patients with OS < 12 months are annotated in each SIG group. Patients' distribution was statistically significant as per χ^2 statistics. Refer to Table 1 for details of *p* values.

(B) Sankey diagram for the longitudinal follow up of patient categorization using the S score in 32 NSCLC patients.

(C) Decision-making tree to calculate the TOPOSCORE. Step 1 consists in calculating the S score (number of SIG2 MGSs present in individual patient stool divided by 45 [frequency (f) SIG2] minus number of SIG1 MGSs present in individual patient stool divided by 37 [frequency (f) SIG1]) + 1 divided by 2. If the S score falls into the gray zone ($0.535 \leq x < 0.791$), the *Akkermansia muciniphila* relative abundance allows to further classify the patient stool as follows: all patients harboring physiological "normal" *A. muciniphila* (Akk) relative abundances ($0 < Akk \leq 4.799$) should be considered OS > 12, while all the other gray zone patients (harboring high Akk levels [Akk^{High}, $Akk \geq 4.8$] and no Akk [Akk0]) have to be considered OS < 12, allowing a final binary categorization into SIG1+ and SIG2+, respectively.

(D) Cox regression univariate analysis and Kaplan-Meier curves of PFS and OS(left and right) in the 245 NSCLC patients according to the binary categorization of the TOPOSCORE gave significant differences ($p = 0.0060$ for PFS, $p < 0.0001$ for OS). Refer to multivariate analyses in Table 1.

(E) Sankey diagram for the longitudinal follow up of patient categorization using the TOPOSCORE in 32 NSCLC patients.

See also Figure S4.

zone (Figure 2A). Of note, 69% of patients with $S \leq 0.5351$ presented an OS < 12 months, contrasting with only 23% of patients with $S \geq 0.7911$ (Figure 2A; Table S3). The Cox regression analysis of the clinical impact of the *S* score on OS confirmed that patients with $S \geq 0.7911$ (henceforth called SIG2) exhibited a significantly prolonged clinical benefit to PD-1 blockade compared with patients falling into the gray zone or $S \leq 0.5351$ (henceforth labeled as SIG1) (Figure S4A). About 22.5%, 31%, and 46.5% of patients in the discovery cohort fell into SIG2, SIG1, and the gray zone, respectively.

Next, we analyzed the intraindividual dynamics of the *S* score in 32 NSCLC patients who were sampled twice, before and within 3 months after treatment start. Interestingly, 33% and 25% of SIG2 and SIG1, respectively, joined the gray zone, while half of patients classified in the gray score shifted to SIG2 and none among the patients changed from gray to SIG1 (Figure 2B). Altogether, 67%, 50%, and 70% of individuals within SIG2, gray, or SIG1 remained in the same category, respectively (Figure 2B). R at 3 months ($n = 12$) were classified either as SIG2 ($n = 8$) or gray ($n = 4$), while NR at this time point ($n = 20$) were either classified as SIG1 ($n = 14$) or gray ($n = 6$).

Refining the prognostic model

To solve the uncertainty of the gray zone, which represented about half of NSCLC patients, we segregated individuals according to the trichotomized distribution of Akk relative abundance (Figure 2C).[31]

Normal levels of Akk ($0 < \text{Akk} \leq 4.799\%$, Akk^{norm}) may be considered as a surrogate of host fitness in comparison with abnormal levels ($\text{Akk} \geq 4.8\%$, Akk^{high}) or the absence of Akk (Akk^{0}).[31] Starting from here, gray zone patients who harbored physiological Akk levels (about 19% of the whole cohort) were incorporated into the SIG2 category (to create the "SIG2+" group), while gray zone patients devoid of (Akk^{0}) or harboring supraphysiologically high Akk levels (23% and 4% of the whole cohort, respectively) were incorporated into the SIG1 category (to create the "SIG1+" group) (Table S3). Thus, based on *S* scoring and Akk levels, we built a final binomial categorical score of immunoresistance-related dysbiosis, which we termed TOPOSCORE, to classify NSCLC patients into two risk categories, which were either SIG2+ (comprising SIG2 patients plus gray zone Akk^{norm} patients) or SIG1+ (encompassing SIG1 patients plus gray zone patients with undetectable or supranormal Akk) (Figure 2C; Table S3). Cox regression analysis confirmed the clinical impact of the TOPOSCORE on PFS and OS. Thus, patients with a SIG2+ TOPOSCORE exhibited a significantly prolonged clinical benefit to PD-1 blockade compared with patients with a SIG1+ TOPOSCORE (Table S3; Figure 2D, left and right panels). Moreover, even after adjusting for established risk factors (age, gender, body mass index, antibiotic use, PD-L1 expression, line of treatment, and ECOG performance status), the TOPOSCORE independently correlated with patient survival in multivariate analyses (Table 1A, HR = 0.47 (0.33–0.67), $p = 0.001$). Finally, the intraindividual dynamics of the TOPOSCORE in the same 32 NSCLC individuals sampled twice (baseline and 3 months) showed the relative stability of the SIG phenotype with 67% and 74% patients remaining in their SIG2+ and SIG1+ category, respectively (Figure 2E).

Scoring validation in lung cancer

We next applied the TOPOSCORE to an NSCLC validation cohort of 254 patients under PD-1 blockade (Table S1). The proportions of patients falling into SIG1, gray Akk^{high}, gray Akk^{0}, gray Akk^{norm}, and SIG2 were approximately similar to those described in the discovery cohort with 29%, 7%, 16%, 21%, and 27%, respectively (Table S3). Here, 44.2% and 22% of patients with $S \leq 0.5351$ (SIG1) and $S \geq 0.7911$ (SIG2), respectively, presented an OS < 12 months (Figure 3A; Table S3). As described above for the discovery cohort, the Cox regression analysis of the association of the TOPOSCORE with PFS and OS validated that the SIG2+ category of patients exhibited a significantly prolonged survival compared with the SIG1+ subgroup (Table S3; Figure 3B, $p = 0.058$ for PFS, $p = 0.0034$ for OS), while the tripartite categorization into SIG1, gray, and SIG2 did not perform well (Figure S4B). Here again, the TOPOSCORE classifier represented an independent and more robust prognosis marker than PD-L1, age, and antibiotics use in multivariate analyses (Table 1, HR = 0.59 (0.36–0.97), $p = 0.041$).

Importantly, when pooling all NSCLC patients from the discovery and validation cohorts with an available PD-L1 immunohistochemical tumor labeling ($n = 344$), we could demonstrate the added value of the TOPOSCORE, not only in PD-L1 negative tumors but also in PD-L1 positive NSCLC patients (Figure 3C, $p = 0.0046$ and p = 0.0032, respectively). The prognostic value of the TOPOSCORE was confirmed for previously treated patients but also treatment-naive individuals receiving anti-PD-1 Ab monotherapy alone or in combination with chemotherapy (Figures 3D and 3E).

Prospective validation of the TOPOSCORE in other cancer cohorts amenable to PD-1 blockade

We next extended the use of the NSCLC-related TOPOSCORE to a prospective cohort pooling 83 RCC (from the ONCOBIOTICS trial) and 133 UC (from the IOPREDI trial) treated with anti-PD-(L)1 Abs in 2$^{\text{nd}}$ L therapy (Table S1), for which baseline samples and >6 months-clinical follow up were available. The percentage of SIG1+ patients in the RCC and UC cohorts was 35% and 57%, respectively (Figure 4A). Pooling all urinary tract malignancies, we found that the proportions of patients falling into SIG1, gray Akk^{high}, gray Akk^{0}, gray Akk^{norm}, and SIG2 were approximately similar to those described in NSCLC with 26.4%, 1.4%, 21%, 24%, and 27.3%, respectively (Table S3). As found in NSCLC, 80% and 36% of RCC+UC patients within SIG1 and SIG2 had an OS < 12 months, respectively (Table S3). The Cox regression analysis of the impact of the TOPOSCORE on PFS and OS confirmed that the SIG1+ subset of patients exhibits reduced clinical benefit compared with the SIG2+ subset (Table S3; Figure 4B, left and right panels, $p = 0.0039$ for PFS and $p < 0.0001$ for OS).

As a control, we computed the co-occurrence network, not just for the 245 NSCLC patients who were first enrolled in ONCOBIOTICS but rather randomly selected within the whole cohort of 499 NSCLC patients, 10 times independently, using the leave-one-out methodology to challenge our first TOPOSCORE, and then validated the latter in the rest of the cohort of NSCLC and RCC+UC. This calculation led to the performances summarized in Table S4A. Hence, none of the alternative algorithms

Table 1. Multivariate analyses of the TOPOSCORE in 499 NSCLC patients (discovery + validation cohorts)

Cox proportional-hazards univariate and multivariate analyses for discovery cohort

Variables	Univariate analysis				Multivariate analysis[a]			
	Groups	Hazard ratio	Confidence interval 95%	*p* value[c]	Groups	Hazard ratio	Confidence interval 95%	*p* value
TOPOSCORE	SIG1+ (*n* = 140)	reference			SIG1+ (*n* = 126)	reference		
	SIG2+ (*n* = 105)	0.471	0.340–0.652	<0.001	SIG2+ (*n* = 88)	0.476	0.334–0.677	<0.001
Age, per year	*n* = 245	1.009	0.994–1.025	0.243	*n* = 214	1.014	0.997–1.031	0.102
BMI	<18 (*n* = 22)	reference	N/A	0.003	<18 (*n* = 20)	reference	N/A	0.002
	18–25 (*n* = 142)	0.537	0.323–0.893	0.017	18–25 (*n* = 124)	0.545	0.324–0.915	0.022
	≥25 (*n* = 81)	0.395	0.230–0.680	0.001	≥25 (*n* = 70)	0.371	0.213–0.646	<0.001
Antibiotics	no (*n* = 189)	reference			no (*n* = 166)	reference		
	yes (*n* = 56)	1.813	1.279–2.579	<0.001	Yes (*n* = 48)	2.262	1.549–3.303	<0.001
ECOG-PS	0–1 (*n* = 174)	reference			0–1 (*n* = 178)	reference		
	≥2 (*n* = 36)	1.441	0.971–2.139	0.069	≥2 (*n* = 36)	1.286	0.857–1.928	0.224
Treatment(s) line(s)	1 (*n* = 50)	reference			not included	N/A	N/A	N/A
	≥2 (*n* = 195)	1.154	0.760–1.751	0.501	N/A	N/A	N/A	N/A
PD-L1	0%–49% (*n* = 60)	reference			not included	N/A	N/A	N/A
	≥50% (*n* = 66)	1.128	0.705–1.803	0.616	N/A	N/A	N/A	N/A
Gender	female (*n* = 78)	reference			not included	N/A	N/A	N/A
	male (*n* = 159)	1.101	0.789–1.537	0.572	N/A	N/A	N/A	N/A

Cox proportional-hazards univariate and multivariate analyses for validation cohort

Variables	Univariate analysis				Multivariate analysis[b]			
	Groups	Hazard ratio	Confidence interval 95%	*p* value[c]	Groups	Hazard ratio	Confidence interval 95%	*p* value
TOPOSCORE	SIG1+ (*n* = 137)	reference			SIG1+ (*n* = 103)	reference		
	SIG2+ (*n* = 117)	0.557	0.374–0.830	0.004	SIG2+ (*n* = 90)	0.595	0.362–0.978	0.041
Age, per year	*n* = 254	1.314	0.894–1.93	0.165	*n* = 193	0.970	0.942–0.999	0.43
BMI	<18 (*n* = 17)	reference		0.075	<18 (*n* = 11)	reference		0.310
	18–25 (*n* = 132)	2.326	0.223–1.744	0.102	18–25 (*n* = 103)	3.108	0.723–13.364	0.128
	≥25 (*n* = 105)	1.604	0.573–4.486	0.368	≥25 (*n* = 79)	2 864	0.651–12.605	0.164
Antibiotics	no (*n* = 217)	reference			no (*n* = 170)	reference		
	yes (*n* = 37)	1.385	0.833–2.302	0.210	yes (*n* = 23)	0.961	0.462–2.001	0.916
ECOG-PS	0–1 (*n* = 104)	reference			0–1 (*n* = 170)	reference		
	≥2 (*n* = 147)	1.631	1.085–2.452	0.019	≥2 (*n* = 23)	2.463	1.199–5.059	0.014
Treatment(s) line(s)	1 (*n* = 98)	reference			1 (*n* = 94)	reference		
	≥2 (*n* = 132)	1.659	1.055–2.607	0.028	≥2 (*n* = 99)	1.275	0.723–2.250	0.401
PD-L1	0%–49% (*n* = 73)	reference			0 (*n* = 104)	reference		
	≥50% (*n* = 145)	0.561	0.356–0.884	0.13	≥50% (*n* = 89)	0.632	0.350–1.141	0.128
Gender	female (*n* = 98)	reference			not included	–	–	–
	male (*n* = 156)	1.040	0.845–1.268	0.694	–	–	–	–

[a]Total patients included=214; missing data: 31; total events: 156

[b]Total patients included=193; missing data: 61; total events: 72

[c]Log-rank test was used to compare the survival of different groups. The *p* values ≤ 25 presented in the table correspond to binary comparison, including for BMI for the following groups, <18 x ≥ 18, 18–25 x < 18 or >25, and ≤ 25 x > 25.

yielded a better performance across all the different cohorts than the first one (although some satisfactory scores were observed and shared common MGSs across each other; Table S4B).

Finally, we applied the TOPOSCORE to healthy individuals (HV) instead of cancer patients, computing the metagenomes of public databases (matching HV with cancer patients based on age, sex, and country of residence) and utilizing the MetaPhlAn 4.0 pipeline. To analyze the differences in the taxonomic stool composition between HV and the advanced NSCLC patients (segregated into OS> or <12 months) described above, we performed PCoA of Bray-Curtis distances on batch-corrected data with MMUPHin (Ma et al. 2022[36]) and normalized/standardized

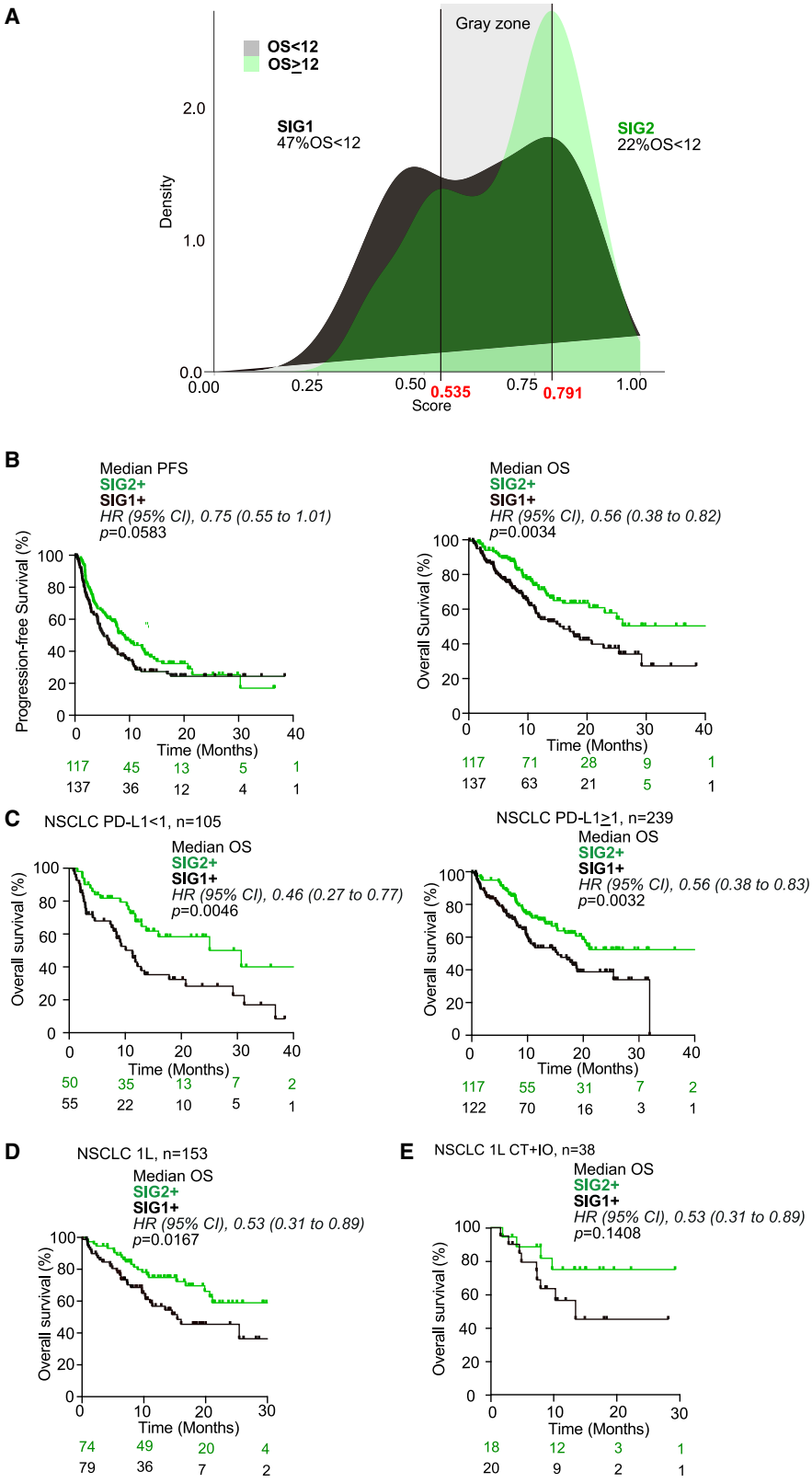

(legend on next page)

data that unveiled significant separation among HV and cancer groups (Figure S5A). To determine the relative contribution of each MGS abundance at baseline to the observed three group separation, MGSs were ordered according to their VIP score, which relied on the supervised PLS-DA (Figure S5B). Not surprisingly, significant MGSs were listed in SIG1 (such as *Enterocloster clostridioformis, E. bolteae, Clostridium symbosium*, etc.) or SIG2 (*Coprococcus comes*, *Dorea longicatena*, etc.). In fact, the *S* score applied to HV (matched for age and geography) highlighted that 68.5% were SIG2, 27.5% fell in the gray zone, and 4% were SIG1. Using the *Akk* trichotomic distribution, we could calculate that approximately 20% of HV are SIG1+ (Figures 4A and S5C).

Altogether, the TOPOSCORE allowed us to conclude that 53%, 58%, 35%, and 57% of 1stL NSCLC, 2ndL NSCLC, 1st+2ndL RCC, and $\geq$2ndL UC patients, respectively, are afflicted by dysbiosis (defined by the SIG1+ phenotype) (Figure 4A) that was associated with immuno- resistance independently of other prognosis factors (Table 1). Thus, the TOPOSCORE represents a robust biomarker correlating with responses to ICIs in patients with lung and genitourinary tract cancers.

Challenging the TOPOSCORE with machine-learning approaches

We assessed the performance of the TOPOSCORE for the identification of NSCLC patients who failed to respond to ICIs in the discovery cohort. The TOPOSCORE showed a sensitivity of 74.1%, specificity of 56.8%, positive predictive value of 69.8%, and negative predictive value of 61.9%, with an AUC of 0.66 (95% confidence interval 0.59–0.73). The TOPOSCORE performance was compared with two machine-learning algorithms. The first, RF via SIAMCAT(REF58), which used the relative abundances of all microbial species, yielded an AUC of 0.651 ± 0.012 in the discovery cohort (Figure S6A). Then, a metagenome-assembled genomes (MAGs)-based RF model was employed, using relative abundances of 141 MAGs with a >95% quality score, which showed stability in interactions across various conditions. This MAGs-based RF model achieved an AUC of 0.65 (95% CI 0.58–0.72) in the same cohort (Figure S6B). Therefore, we conclude that the machine-learning algorithms provided similar degrees of accuracy to foretell individual resistance to ICIs as the TOPOSCORE in the discovery cohort.

Functional pathways associated with SIG1 and SIG2 MGSs

To explore putative microbial functions underlying SIG1 and SIG2 compositions, we analyzed MG pathways by means of the HUMAnN 3.0 pipeline. This pipeline first annotates microbial-specific gene hits according to the Kyoto Encyclopedia of Genes and Genomes (KEGG) orthology and then reconstructs microbial metabolic pathways using the MetaCyc hierarchy. We thus retrieved 664 pathways (unclassified excluded and 441 at 20% prevalence cutoff) in the whole cohort of 499 NSCLC patients, with 11 and 57 pathways exclusively present in SIG1- and SIG2-associated microbial communities, respectively, and 76 shared pathways for a total of 144 pathways (Figure S6C; Table S5A). PLS-DA ordination plots showed significant compositional differences in the functional pathways across sample types among SIG1+ and SIG2+ patients, while the VIP plot showed discriminant and significant pathways for each cohort (Figures S6D and S6E). SIG2 metabolic functions encompass sulfur oxidation, tRNA charging and processing, stachyose and mannan degradation, L-glutamate and L glutamine as well as L-arginine and L-ornithine biosynthesis, L-tryptophane and dTDP-L-rhamnose biosynthesis, as well as the pentose phosphate pathways (Tables S5A and S5B). By contrast, SIG1 metabolic functions comprise fatty acid beta-oxidation, 5′deoxyadenosine and L phenylalanine degradation, purine and L-histidine degradation, and guanosine and L-lysine biosynthesis (Tables S5A and S5B). A hierarchical clustering based on the overall 144 pathway abundances related to SIG1 and SIG2 MGSs, was applied to the 499 NSCLC patients, showing a clear separation of patients into two distinct groups, cluster 1 harboring 73% of SIG1+ individuals enriched in SIG1 functional pathways and cluster 2 harboring 70% of SIG2+ patients enriched in SIG2 functional pathways (χ^2 statistic with Yates correction = 88.305, $p < 0.00001$) (Figure S6F; Table S5C). Thus, even though 76 pathways are shared among the SIG1 and SIG2 groups of microbial species, the overall distribution of 144 pathways mirrored the seesaw balance between these interactive groups, dividing them into two distinct functional patterns related to SIG1 and SIG2 MGS functions (Fisher's exact test < 0.00001).

Development of a user-friendly qPCR-based assay

To transform the TOPOSCORE into a clinically actionable diagnosis tool, we considered circumventing the costly, laborious, and time-consuming method of shotgun metagenomics by means of a qPCR-based assay that can be performed within 48 h for determining the prevalence of bacteria. Based on the most prevalent MGSs found for the gut oncomicrobial signatures across various cohorts[22,23] and the feasibility of designing bacteria-specific and reliable probe sets (Figure S7), we focused our qPCR-based assay on 15 SIG2- and 5 SIG1-associated bacteria, as well as on *Akkermansia spp.* (Figure S8; Table S6).

First, we re-ran the TOPOSCORE calculation for the whole NSCLC cohort based on the MGS-based relative abundances

Figure 3. Performance of the TOPOSCORE in the validation cohort of NSCLC patients

(A) As for Figure 1A (discovery cohort), we applied the same calculation model and the same boundaries of the S score distribution in the validation cohort of 254 NSCLC patients by means of Kernel density estimation (KDE) and annotated the % of patients with OS < 12 in each group. Refer to Table S3 for statistical analyses. Refer to Figure S4 for Kaplan-Maier curves according to the S score.

(B) Cox regression univariate analysis and Kaplan-Meier curves of PFS and OS in the 254 NSCLC patient validation cohort according to the TOPOSCORE gave significant differences ($p = 0.0583$ for PFS, $p = 0.0034$ for OS). Refer to multivariate analyses in Table 1.

(C–E) Idem as in (B) but taking into account both NSCLC cohorts to analyze the effects of the TOPOSCORE on OS according to tumor PD-L1 expression (C, $p = 0.0046$ for PD-L1 < 1 and $p = 0.0032$ for PD-L1 $\geq$ 1) or focusing on first-line immunotherapy (D, $p = 0.0167$) or first-line chemo-immunotherapy (E, $p = 0.1408$).

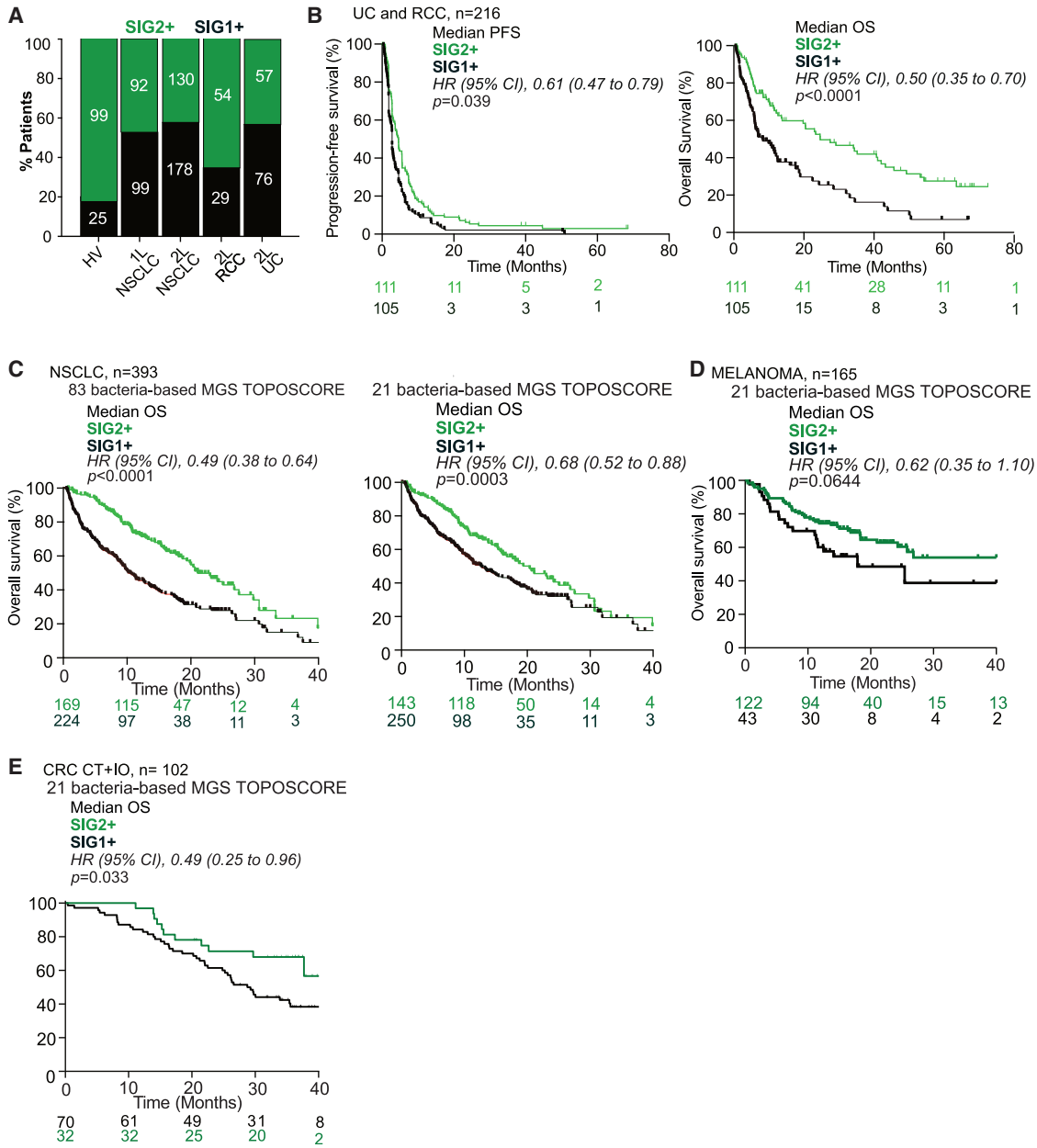

Figure 4. Validation of the TOPOSCORE across malignancies

(A) Bar graph recapitulating the proportion of individuals (French adult HV or cancer patients) diagnosed with a gut dysbiosis (defined as SIG1+ using TOPOSCORE) according to histotype, and treatment line (also refer to Figure S5C).

(B) Application of the TOPOSCORE in a prospective cohort of 133 UC and 83 RCC patients in Cox regression analyses and Kaplan-Meier curves of survival (PFS, $p = 0.0039$ and OS, $p < 0.0001$). Refer to Table S3.

(C) Cox regression analysis and Kaplan-Meier survival curves in 393 NSCLC patients according to the 83 (left, $p < 0.0001$) versus 21 (right, $p = 0.0003$) MGS-based TOPOSCORE based on shotgun MG data.

(D) Implementation of the 21 MGS-based TOPOSCORE in a retrospective cohort of 165 melanoma patients (Lee et al.[25]). Kaplan-MeierOS curves are depicted for SIG1+ versus SIG2+ melanoma patients ($p = 0.0644$).

(E) Implementation of the 21 MGS-based TOPOSCORE in a retrospective cohort of colorectal cancer (CRC) patients enrolled in the open-label phase 2 trial ATEZOTRIBE (Antoniotti et al. ASCO 2023[35]) and treated with chemoimmunotherapy (left, $n = 102$). Kaplan-MeierOS are depicted for SIG1+ versus SIG2+ CRC. Cox's proportional-hazards analysis and log rank tests were applied for all Kaplan-Meier curves ($p = 0.033$).

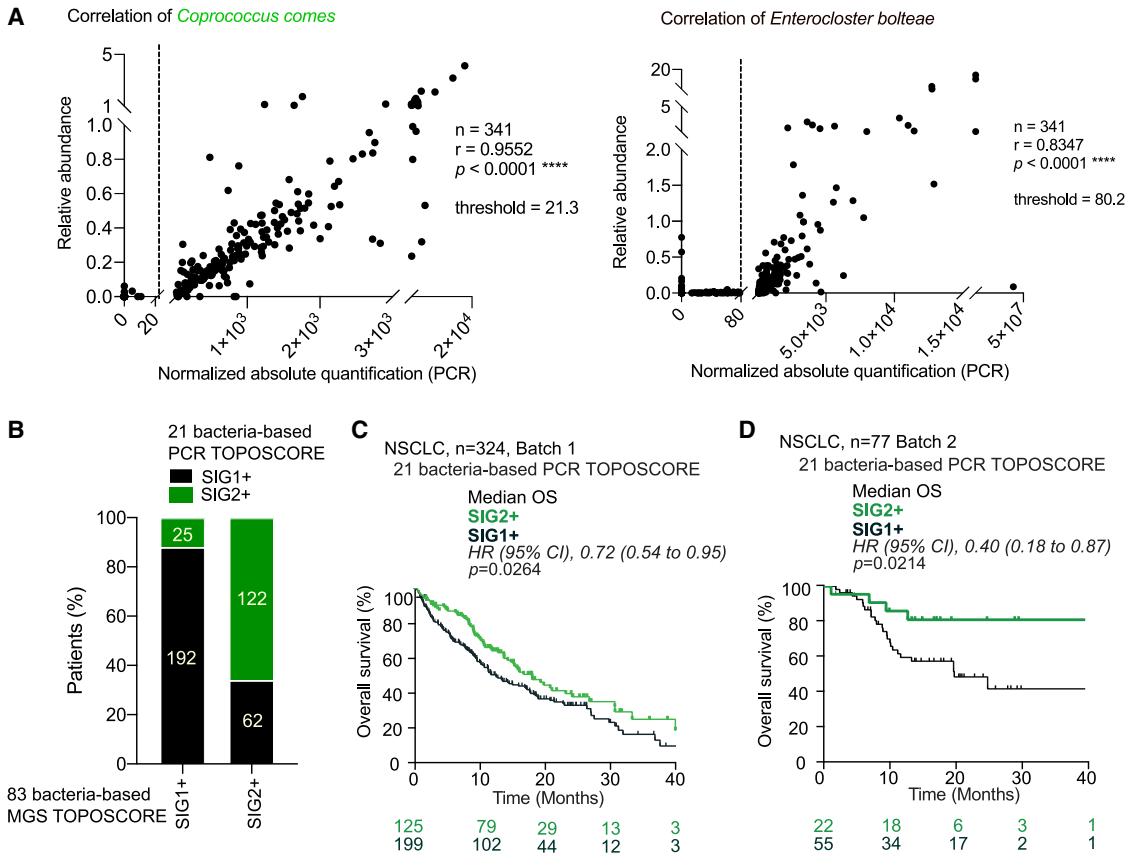

Figure 5. A user-friendly qPCR-based TOPOSCORE

(A) Prototypic examples of two Spearman correlations between qPCR and shotgun MG-based bacterial relative abundances (also refer to Figure S8) gave significant results (*Coprococcus comes* $p < 0.0001$, *Enterocloster bolteae* $p < 0.0001$)

(B) Consistencies between 21-qPCR-based and 83 MGS-based TOPOSCORE to determine SIG1+ versus SIG2+ categorization in the cohort of 401 NSCLC patients evaluable both methods.

(C and D) Cox regression analysis and Kaplan-Meier survival curves using qPCR-based determination of bacterial abundance using the 21 MGS-based TOPOSCORE in a first batch of 324 fecal sample DNA from NSCLC patients (C, $p = 0.0264$) and in a subsequent cohort of 77 NSCLC patients (batch 2, D, $p = 0.0214$) (also refer to Figures S7 and S8 and Table S6).

of these 21 microbial species (instead of the full set of 83 bacteria). In Figure 4C, we show the survival curve of the 393 NSCLC patients, confirming that the 83 MGS-based TOPOSCORE separates patients with a favorable versus dismal prognosis (left panel). A comparable performance was obtained using the reduced 21 MGS-based TOPOSCORE determined by shotgun MG analyses (Figure 4C, right panel). The 21 MGS-based TOPOSCORE was validated in an external cohort of 165 melanoma patients already described.[25] Using the 21 MGS-based TOPOSCORE, we observed that the 43 patients classified as SIG1+ tended to have a shorter OS ($p = 0.06$) than the 122 patients classified as SIG2+ (Figure 4D).

Lastly, we also challenged the TOPOSCORE in 102 colorectal cancer patients enrolled in the chemoimmunotherapy arm of the open-label phase II "ATEZOTRIBE" trial.[35,37] Here again, the 21-MGS-based TOPOSCORE was associated with OS (Figure 4E).

Next, we analyzed correlative patterns to score the relative abundance of fecal bacteria with the two methods (shotgun MG versus qPCR) and to classify patients into SIG1+ versus SIG2+ categories. First, the relative abundances determined by MGSs and PCR of each of the 21 bacterium-specific DNA exhibited high Spearman correlation coefficients, validating the switch from shotgun MG to qPCR (Figure 5A to exemplify *C. comes* and *E. bolteae*, Figure S8 for the other 19 bacteria). Second, there was 78% matching between the categorization into SIG1+ versus SIG2+ patients based on the 83-MGS-based signature and the 21 qPCR-based TOPOSCORE (87/401 patients were inconsistently classified, Figure 5B). Third, when utilizing the 21 bacterium-specific PCR probe sets on the remaining fecal DNA (originally extracted for shotgun MG) from the whole NSCLC cohort ($n = 324$), we confirmed that the 21 qPCR-based assay dichotomized patients into two groups with significantly different OS (SIG1 < SIG2) (Figure 5C, $p = 0.0264$). Fourth, we validated the robustness of the qPCR-based assay in a prospective cohort of 77 NSCLC patients (Figure 5D, $p = 0.0214$).

In conclusion, we demonstrated that a rapid PCR-based test that can be easily translatable into clinical routine, reliably

stratified NSCLC patients amenable to immunotherapy with a better prognosis.

DISCUSSION

Despite the use of microbiome-trained machine-learning across different geographical cohorts, consistent prediction of PD-(L)1 therapy outcomes remains elusive. Notably, there has not been a reproducible microbiome signature to reliably stratify patients individually. This observation is consistent with three meta-analyses spanning various cancer types and therapies that failed to resolve discrepancies in existing cohorts.[38–40] Recently, two meta-analyses focused on melanoma utilized shotgun MG databases and machine-learning methodology to offer partial clarity on the "microbiotypes" associated with responses or resistance to immunotherapy.[25,26]

In this study, we chose an ecosystem-based strategy. Hence, our work suggests gut residence of cooperative ecosystems yielding consistent co-abundance patterns harboring opposite clinical relevance (sensitivity versus resistance to ICIs) in a seesaw manner. Computing the TOPOSCORE on 920 advanced cancer patients, we found that approximately 50% of individuals could be classified as SIG1+ among whom 63% exhibited an OS < 12 months.

The prevalence of bacteria from the SIG1 cluster is lower than that of bacteria from the SIG2 cluster. Thus, ~50% of SIG1 MGSs have a prevalence <15%, while ~55% of SIG2 MGSs have a prevalence >50% in both HV and cancer patients (Figure S6). SIG1 contained 37 species belonging to the *Enterocloster* genus, *Streptococcaceae*, *Veillonellaceae*, and *Lactobacillaceae* families, already identified in immune-resistant patients.[2,16,18,20] In fact, SIG1 comprises many microbial components of the oral cavity that can transit from the supraglottic compartment down to the bronchoalveolar space or the small intestine, as a result of pH fluctuations, comedications (proton pump inhibitors), or dysphagia.[25,32,41–43] Oralization of the intestinal microbiota has been linked to the failure of immunotherapy and immune-related adverse events.[26,44–46] *Veillonella spp.* have the capacity to expand TH17 pro-angiogenic and pro-oncogenic lymphocytes that contribute to dismal prognosis and resistance to cytotoxicants in NSCLC.[32] The *Enterocloster* genus (*E. aldensis*, *E. asparagiformis*, and *E. bolteae*) represents a vancomycin-sensitive clade of immunosuppressive bacteria, dominant in the intestinal microbiota of people and patients suffering from aging and chronic inflammatory disorders including cancer.[39,47] By causing a beta-adrenergic receptor-dependent stress ileopathy and an *Enterocloster* genus-dominated dysbiosis, some malignancies (and other pathological disorders such as stroke) may increase gut permeability, favoring translocation of inflammatory mediators and bacteremia with immunosuppressive potential.[4,48] Interestingly, the gut microbiome health index (GMHI), an index proposed to predict the disease likelihood of an individual based on its fecal microbial composition[49] found species in the non-healthy group similar to the ones retrieved here in SIG1 (see https://github.com/jaeyunsung/GMHI_2020/blob/master/MN_species.txt). Instead, SIG2 was composed of 45 species gathering *Lachnospiraceae* and *Oscillospiraceae* family members that are strongly associated with healthy status and favorable clinical responses.[4,8,17,26,50,51] Indeed, functional fingerprints of SIG2 (such as stachyose degradation,[17] biosynthesis of L-ornithine and L-Arginine within the polyamine pathway,[52–55] purine ribonucleoside degradation[56]) suggest metabolic patterns that favor tumor cell cycle control and immunosurveillance.

Sensitivity, specificity, positive and negative predictive values of the 83 MGS TOPOSCORE applied to NSCLC were 74.1%, 56.8%, 69.8%, and 61.9%, respectively, with an AUC = 0.66 [95% confidence interval 0.59–0.73]. Of note, the alternative state-of-the-art machine-learning algorithms (including SIRUS, SIAMCAT, and MAGs-based RF) performed equally well (Figure S5). The robustness of the TOPOSCORE was not only illustrated for patients with NSCLC but also in patients with stage IV urinary tract amenable to ICI (including 83 (1L + 2L) RCC and 133 (>2L) UC. Interestingly, the fraction of SIG1+ patients was lower in RCC (34%) than in UC (57%), suggesting that the 1st L treatment (mostly kinase inhibitors in RCC and platinum-based chemotherapy in UC) may influence the incidence of dysbiosis.

Longitudinal scoring of patients will be instrumental to understand the impact of therapeutic interventions on gut homeostasis. It remains to be established whether the 83 MGS TOPOSCORE may be extended and applied to other types of malignancies (that may be influenced by extraintestinal microbiota). At the speculative level, the TOPOSCORE might become a valuable tool to select donors of FMT and hence to exclude the 20% of HV falling into the SIG1+ category and instead prioritize the ~17% HV with a particularly favorable TOPOSCORE ($\geq$0.90). Of note, in contrast to HV, only 6% cancer patients (43/715) scored $\geq$0.90. The TOPOSCORE also covers the unmet medical need of patient stratification based on intestinal dysbiosis in order to ascribe resistance to ICIs to an objective deviation from the healthy taxonomic composition (rather than to cancer cell-intrinsic molecular cues) and to guide microbiota-centered interventions. Hence, the TOPOSCORE represents a potentially actionable diagnosis tool for the pharmacodynamics of live biotherapeutics, FMT, and prebiotics. More specifically, the TOPOSCORE offers a user-friendly process to rapidly evaluate gut dysbiosis in a given individual at any time of the disease. Indeed, we showed that it was possible to replace the 83 MGS-based shotgun MG TOPOSCORE by a 21-bacteria-probe set-based qPCR with 78% consistency. Hence, pending further optimization, this 21-bacteria-based qPCR assay may be considered as a proxy of the TOPOSCORE.

Limitations of the study

This study has some limitations. The TOPOSCORE may fluctuate with patient accrual, cancer histotype selection, the clinical endpoint, and geography. Inclusion of additional MGSs into the qPCR-based TOPOSCORE may improve its performance. We could not verify the stability of the TOPOSCORE at baseline, before treatment, by performing serial sampling. Longitudinal analyses have been performed before and after treatment only. The MG-to-PCR-switch of the TOPOSCORE has been biased by the availability of bacteria-specific probe sets and bacterial isolation techniques. Finally, the TOPOSCORE may misestimate the frequency of dysbiosis in healthy volunteers because such

volunteers were matched with cancer patients based on age, sex, and geography but not based on diet and comedications. The TOPOSCORE does not allow to distinguish the prognostic versus predictive nature of the impact of the intestinal microbiota composition on OS. Future studies with large effect sizes will be required to answer this question.

STAR★METHODS

Detailed methods are provided in the online version of this paper and include the following:

- KEY RESOURCES TABLE
- RESOURCE AVAILABILITY
  - Lead contact
  - Materials availability
  - Data and code availability
- STUDY PARTICIPANT DETAILS
  - Patient cohorts and specimen
- METHOD DETAILS
  - Shotgun metagenomics sequencing and bioinformatic analysis
  - Statistical analysis of metagenomic data
  - Toposcore algorithm
  - Machine learning approach for responsiveness to immunotherapy
  - Gene Pathway Functional analyses
  - qPCR-based TOPOSCORE using Precision Microbiome Profiling (PMP™)
- ADDITIONAL RESOURCES
  - Clinical trial registry numbers

SUPPLEMENTAL INFORMATION

Supplemental information can be found online at https://doi.org/10.1016/j.cell.2024.05.029.

ACKNOWLEDGMENTS

We would like to particularly thank the patients who participated in the clinical trial and distinct employees at the Gustave Roussy Cancer Campus, in particular Maria Semedo de Brito, Marzieh Jenabi, and Melanie Boulhic who helped in the connections between patients and clinicians.

L. Zitvogel, C.S., and L.D. were supported by the French Ministry of Health PIA5, ANR, program RHU5 "ANR-21-RHUS-0017" IMMUNOLIFE" title: "effects of antibiotics on the clinical outcome to immunotherapy." L. Zitvogel, C.A.C.S., and L.D. were supported by the European Union's Horizon 2020 research and innovation programme under grant agreement number: 964590, project acronym: IHMCSA, project title: International Human Microbiome Coordination and Support Action. L. Zitvogel., N.S., G.P., L.D., V.I., and B.R. were supported by European Union's Horizon 2020 research and innovation programme under grant agreement number: 825410, project acronym: ONCOBIOME, project title: Gut OncoMicrobiome Signatures (GOMS) associated with cancer incidence, prognosis, and prediction of treatment response. L.D., L. Zitvogel, and M.F. were supported by the European Union's Horizon Europe research and innovation programme under grant agreement number 101095604—(project acronym: PREVALUNG EU, project title: Biomarkers affecting the transition from cardiovascular disease to lung cancer: toward stratified interception). L. Zitvogel also received an ANR grant—French-German Ileobiome—19-CE15-0029-01. L. Zitvogel and G.K. received a donation from Seerave Foundation. L. Zitvogel, L.D., and E.D. were supported by the SIRIC Stratified Oncology Cell DNA Repair and Tumor Immune Elimination (SOCRATE). L. Zitvogel and L.D. were supported by SIGN'IT ARC foundation, project acronyms: MICROBIONT-PREDICT (2021) and Made-IT (2023). L. Zitvogel and G.K. were supported by the Ligue contre le Cancer (équipe labelisée); ANR Projets blancs; ANR under the frame of E-Rare-2, the ERA-Net for Research on Rare Diseases; Association pour la recherche sur le cancer (ARC); Bristol-Myers Squibb Company (International Immuno-Oncology Network), Cancéropôle Ile-de-France; Chancellerie des universités de Paris (Legs Poix), Fondation pour la Recherche Médicale (FRM); a donation by Elior; the European FP7 programme (ArtForce, grant agreement number: 257144); the European Research Council (ERC-2021-AdG, project: ICD-Cancer, grant agreement number: 101052444); Fondation Carrefour; Institut National du Cancer (INCa); Inserm (HTE); Institut Universitaire de France; LeDucq Foundation; the LabEx Immuno-Oncology; FHU CARE, Dassault, and Badinter Philantropia, and the Paris Alliance of Cancer Research Institutes (PACRI). A.C. is supported by the CPRIT Research Training Program (RP170067). The qPCR (PMP™) work was supported by grant no 310142 from the Norwegian Research Council. F.A. was supported by the Agence Nationale de la Recherche under grant number ANR-18-IBHU-0002. N.S. was supported by the European Research Council (ERC-STG project MetaPG-716575); MIUR 'Futuro in Ricerca' (grant no. RBFR13EWWI_001) to N.S.; the European H2020 program (ONCOBIOME-825410 project and MASTER-818368 project); the National Cancer Institute of the National Institutes of Health (1U01CA230551); and the Premio Internazionale Lombardia e Ricerca 2019 to G.K. The bladder cancer cohort of patients allowing the IOPREDI / STRONG ancillary study (NCT03084471) biobanking and data mining was funded by AstraZeneca. C.A.C. was founded by MSD Avenir. C.C. received a grant from Regione Toscana Bando Salute named IN BILICO that partially supported AtezoTRIBE Trial. The funders had no role in the design of the study, in the writing of the manuscript, or in the decision to publish the results.

AUTHOR CONTRIBUTIONS

Conceptualization: L.D., V.I., and L. Zitvogel; methodology: V.I., G.W., L. Zhao, J.W., and N.S.; software: V.I., G.P., A.M.T., G.W., L.L., N.Z., L. Zha, J.W., and N.S.; validation: V.I., G.P. G.W., L.L., L. Zha, J.W., and N.S.; formal analysis: V.I., G.P., L.L., C.T., R.B., and J.W.; investigation: L.D., C.A.C.S., C.S., I.D., S.Z., P.L., A.R., R.D., M.F., and M.M.; resources: F.B., B.E., B.B., L.A., D.P., F.A., L.P., A.F., M.L.I., E.D., K.A.L., L.A.B., J.R.B., R.K.W., B.R., F.M., C.C., G.Z., S.F., J.M., C.A.-V., D.M.-S., F. Goldwasser, A.S., E.P., F. Ghiringhelli, N.B., and S.M.; data curation: L.D., C.A.C.S., and V.I.; writing—original draft: L.D., V.I., G.K., and L. Zitvogel; writing—review & editing: all but in particular L.D., V.I., C.A.C.S., G.K., and L. Zitvogel; visualization: L.D., V.I., C.A.C.S., and R.B.; supervision: L.D., N.S., G.K., and L. Zitvogel; project administration, L.D. and L. Zitvogel; funding acquisition: L.D., G.K., and L. Zitvogel.

DECLARATION OF INTERESTS

L. Zitvogel is founder of everImmune and its SAB President. L.D. is an everImmune SAB member. R.D. is a scientific co-founder of everImmune. L. Zitvogel received a research contract from Kaleido, 9 meters/Innovate Pharma, and is currently sponsored by Pileje. G.Z. received a research grant from Fondation Roche; received fees from Roche, MSD, BMS, and Astra Zeneca; and is a consultant for Da Volterra & Inventiva. E.D. reports grants and personal fees from Roche Genentech, grants from Boehringer, grants from AstraZeneca, grants and personal fees from Merck Serono, grants from BMS, and grants from MSD. E.D. is founder of Graegis/Alys. M.L.I., L.B., and A.F. are employees and shareholders of Bio-Me. P.D. had consulting and advisory roles for AstraZeneca, Bristol-Myers Squibb, Boehringer Ingelheim, Celgene, Daiichi Sankyo, Eli Lilly, Merck, Novartis, Pfizer, prIME Oncology, Peer CME, Roche, and Samsung, as well as honoraria from AstraZeneca, Bristol-Myers Squibb, Boehringer Ingelheim, Celgene, Eli Lilly, Merck, Novartis, Pfizer, prIME Oncology, Peer CME, Roche, and Samsung. P.D. ran clinical trials as principal or co-investigator for AstraZeneca, Bristol-Myers Squibb, Boehringer Ingelheim, Eli Lilly, Merck, Novartis, Pfizer, Roche, MedImmune, Sanofi-Aventis, Taiho Pharma, Novocure, and Daiichi Sankyo and received travel, accommodation, and expenses from AstraZeneca, Roche, Novartis, prIME Oncology, and Pfizer. M.F. and R.K.W. were supported by the Seerave Foundation. R.K.W. received unrestricted research grants from Takeda, J&J, Ferring, and Tramedico; speaker's fee from AbbVie, MSD., and Boston Scientific; and has acted as consultant for Takeda Pharmaceuticals. C.C. reported personal fees from Amgen, Bayer, Merck Serono, MSD, Nordic Pharma, Roche, Pierre Fabre, Servier, and Takeda and research grants from Bayer, Merck Serono,

Pierre Fabre, Seagen, Servier, and Tempus. F.G. received honoraria from Amgen, Sanofi, Merk Serono, MSD, BMS, and Astra Zeneca; had a consultancy or advisory role for Roche and Enterome; and received direct research fundings from Roche, Enterome, Astra Zeneca, and Servier and traveling supports from Servier, Amgen, and Roche. L. Zaho is cofounder of Notitia Biotechnologies. F.B. institutional interest AbbVie, ACEA, Amgen, Astra Zeneca, Bayer, Bristol-Myers Squibb, Boehringer Ingelheim, EISAI, Eli Lilly Oncology, F. Hoffmann–La Roche Ltd, Genentech, Ipsen, Ignyta, Innate Pharma, Loxo, Novartis, MedImmune, Merck, Mirati, MSD, Pierre Fabre, Pfizer, Sanofi-Aventis, and Takeda.art

Received: August 30, 2023
Revised: January 16, 2024
Accepted: May 14, 2024
Published: June 20, 2024

REFERENCES

1. Cho, I., and Blaser, M.J. (2012). The human microbiome: at the interface of health and disease. Nat. Rev. Genet. *13*, 260–270. https://doi.org/10.1038/nrg3182.
2. Gilbert, J.A., Blaser, M.J., Caporaso, J.G., Jansson, J.K., Lynch, S.V., and Knight, R. (2018). Current understanding of the human microbiome. Nat. Med. *24*, 392–400. https://doi.org/10.1038/nm.4517.
3. Gacesa, R., Kurilshikov, A., Vila, V.A., Sinha, T., Klaassen, M., Gacesa, R., Kurilshikov, A., Vich Vila, A., Sinha, T., Klaassen, M.A.Y., Bolte, L.A., Andreu-Sánchez, S., Chen, L., Collij, V., Hu, S., et al. (2022). Environmental factors shaping the gut microbiome in a Dutch population. Nature *604*, 732–739. https://doi.org/10.1038/s41586-022-04567-7.
4. Yonekura, S., Terrisse, S., Alves Costa Silva, C.A.C., Lafarge, A., Iebba, V., Ferrere, G., Goubet, A.-G., Fahrner, J.-E., Lahmar, I., Ueda, K., et al. (2022). Cancer induces a stress ileopathy depending on B-adrenergic receptors and promoting dysbiosis that contribute to carcinogenesis. Cancer Discov. *12*, 1128–1151. https://doi.org/10.1158/2159-8290.CD-21-0999.
5. Davar, D., Dzutsev, A.K., McCulloch, J.A., Rodrigues, R.R., Chauvin, J.-M., Morrison, R.M., Deblasio, R.N., Menna, C., Ding, Q., Pagliano, O., et al. (2021). Fecal microbiota transplant overcomes resistance to anti–PD-1 therapy in melanoma patients. Science *371*, 595–602. https://doi.org/10.1126/science.abf3363.
6. Baruch, E.N., Youngster, I., Ben-Betzalel, G., Ortenberg, R., Lahat, A., Katz, L., Adler, K., Dick-Necula, D., Raskin, S., Bloch, N., et al. (2021). Fecal microbiota transplant promotes response in immunotherapy-refractory melanoma patients. Science *371*, 602–609. https://doi.org/10.1126/science.abb5920.
7. Routy, B., Le Chatelier, E., Derosa, L., Duong, C.P.M., Alou, M.T., Daillère, R., Fluckiger, A., Messaoudene, M., Rauber, C., Roberti, M.P., et al. (2018). Gut microbiome influences efficacy of PD-1-based immunotherapy against epithelial tumors. Science *359*, 91–97. https://doi.org/10.1126/science.aan3706.
8. Gopalakrishnan, V., Spencer, C.N., Nezi, L., Reuben, A., Andrews, M.C., Karpinets, T.V., Prieto, P.A., Vicente, D., Hoffman, K., Wei, S.C., et al. (2018). Gut microbiome modulates response to anti-PD-1 immunotherapy in melanoma patients. Science *359*, 97–103. https://doi.org/10.1126/science.aan4236.
9. Derosa, L., Routy, B., Fidelle, M., Iebba, V., Alla, L., Pasolli, E., Segata, N., Desnoyer, A., Pietrantonio, F., Ferrere, G., et al. (2020). Gut Bacteria Composition Drives Primary Resistance to Cancer Immunotherapy in Renal Cell Carcinoma Patients. Eur. Urol. *78*, 195–206. https://doi.org/10.1016/j.eururo.2020.04.044.
10. Zitvogel, L., Ma, Y., Raoult, D., Kroemer, G., and Gajewski, T.F. (2018). The microbiome in cancer immunotherapy: Diagnostic tools and therapeutic strategies. Science *359*, 1366–1370. https://doi.org/10.1126/science.aar6918.
11. Smith, C.C., Beckermann, K.E., Bortone, D.S., De Cubas, A.A., Bixby, L.M., Lee, S.J., Panda, A., Ganesan, S., Bhanot, G., Wallen, E.M., et al. (2018). Endogenous retroviral signatures predict immunotherapy response in clear cell renal cell carcinoma. J. Clin. Invest. *128*, 4804–4820. https://doi.org/10.1172/JCI121476.
12. Vétizou, M., Pitt, J.M., Daillère, R., Lepage, P., Waldschmitt, N., Flament, C., Rusakiewicz, S., Routy, B., Roberti, M.P., Duong, C.P.M., et al. (2015). Anticancer immunotherapy by CTLA-4 blockade relies on the gut microbiota. Science *350*, 1079–1084. https://doi.org/10.1126/science.aad1329.
13. Hojo, M., Asahara, T., Nagahara, A., Takeda, T., Matsumoto, K., Ueyama, H., Matsumoto, K., Asaoka, D., Takahashi, T., Nomoto, K., et al. (2018). Gut Microbiota Composition Before and After Use of Proton Pump Inhibitors. Dig. Dis. Sci. *63*, 2940–2949. https://doi.org/10.1007/s10620-018-5122-4.
14. Kulkarni, A., Kumar, M., Pease, D.F., Wang, Y., DeFor, T.E., and Patel, M. (2019). Impact of antibiotics and proton pump inhibitors on clinical outcomes of immune check point blockers in advanced non-small cell lung cancers and metastatic renal cell cancer. J. Clin. Oncol. *37*, e20520. https://doi.org/10.1200/JCO.2019.37.15_suppl.e20520.
15. Derosa, L., Routy, B., Kroemer, G., and Zitvogel, L. (2018). The intestinal microbiota determines the clinical efficacy of immune checkpoint blockers targeting PD-1/PD-L1. Oncoimmunology *7*, e1434468. https://doi.org/10.1080/2162402X.2018.1434468.
16. Derosa, L., Hellmann, M.D., Spaziano, M., Halpenny, D., Fidelle, M., Rizvi, H., Long, N., Plodkowski, A.J., Arbour, K.C., Chaft, J.E., et al. (2018). Negative association of antibiotics on clinical activity of immune checkpoint inhibitors in patients with advanced renal cell and non-small-cell lung cancer. Ann. Oncol. *29*, 1437–1444. https://doi.org/10.1093/annonc/mdy103.
17. Spencer, C.N., McQuade, J.L., Gopalakrishnan, V., McCulloch, J.A., Vetizou, M., Cogdill, A.P., Khan, M.A.W., Zhang, X., White, M.G., Peterson, C.B., et al. (2021). Dietary fiber and probiotics influence the gut microbiome and melanoma immunotherapy response. Science *374*, 1632–1640. https://doi.org/10.1126/science.aaz7015.
18. Mager, L.F., Burkhard, R., Pett, N., Cooke, N.C.A., Brown, K., Ramay, H., Paik, S., Stagg, J., Groves, R.A., Gallo, M., et al. (2020). Microbiome-derived inosine modulates response to checkpoint inhibitor immunotherapy. Science *369*, 1481–1489. https://doi.org/10.1126/science.abc3421.
19. Roberti, M.P., Yonekura, S., Duong, C.P.M., Picard, M., Ferrere, G., Tidjani Alou, M., Rauber, C., Iebba, V., Lehmann, C.H.K., Amon, L., et al. (2020). Chemotherapy-induced ileal crypt apoptosis and the ileal microbiome shape immunosurveillance and prognosis of proximal colon cancer. Nat. Med. *26*, 919–931. https://doi.org/10.1038/s41591-020-0882-8.
20. Overacre-Delgoffe, A.E., Bumgarner, H.J., Cillo, A.R., Burr, A.H.P., Tometich, J.T., Bhattacharjee, A., Bruno, T.C., Vignali, D.A.A., and Hand, T.W. (2021). Microbiota-specific T follicular helper cells drive tertiary lymphoid structures and anti-tumor immunity against colorectal cancer. Immunity *54*, 2812–2824.e4. https://doi.org/10.1016/j.immuni.2021.11.003.
21. Goubet, A.-G., Lordello, L., Alves Costa Silva, C., Peguillet, I., Gazzano, M., Mbogning-Fonkou, M.D., Thelemaque, C., Lebacle, C., Thibault, C., Audenet, F., et al. (2022). Escherichia coli-Specific CXCL13-Producing TFH Are Associated with Clinical Efficacy of Neoadjuvant PD-1 Blockade against Muscle-Invasive Bladder Cancer. Cancer Discov. *12*, 2280–2307. https://doi.org/10.1158/2159-8290.CD-22-0201.
22. Park, E.M., Chelvanambi, M., Bhutiani, N., Kroemer, G., Zitvogel, L., and Wargo, J.A. (2022). Targeting the gut and tumor microbiota in cancer. Nat. Med. *28*, 690–703. https://doi.org/10.1038/s41591-022-01779-2.
23. Thomas, A.M., Fidelle, M., Routy, B., Kroemer, G., Wargo, J.A., Segata, N., and Zitvogel, L. (2023). Gut OncoMicrobiome Signatures (GOMS) as next-generation biomarkers for cancer immunotherapy. Nat. Rev. Clin. Oncol. *20*, 583–603. https://doi.org/10.1038/s41571-023-00785-8.

24. Newsome, R.C., Gharaibeh, R.Z., Pierce, C.M., da Silva, W.V., Paul, S., Hogue, S.R., Yu, Q., Antonia, S., Conejo-Garcia, J.R., Robinson, L.A., et al. (2022). Interaction of bacterial genera associated with therapeutic response to immune checkpoint PD-1 blockade in a United States cohort. Genome Med. *14*, 35. https://doi.org/10.1186/s13073-022-01037-7.

25. Lee, K.A., Thomas, A.M., Bolte, L.A., Björk, J.R., de Ruijter, L.K., Armanini, F., Asnicar, F., Blanco-Miguez, A., Board, R., Calbet-Llopart, N., et al. (2022). Cross-cohort gut microbiome associations with immune checkpoint inhibitor response in advanced melanoma. Nat. Med. *28*, 535–544. https://doi.org/10.1038/s41591-022-01695-5.

26. McCulloch, J.A., Davar, D., Rodrigues, R.R., Badger, J.H., Fang, J.R., Cole, A.M., Balaji, A.K., Vetizou, M., Prescott, S.M., Fernandes, M.R., et al. (2022). Intestinal microbiota signatures of clinical response and immune-related adverse events in melanoma patients treated with anti-PD-1. Nat. Med. *28*, 545–556. https://doi.org/10.1038/s41591-022-01698-2.

27. Zhang, C., Yin, A., Li, H., Wang, R., Wu, G., Shen, J., Zhang, M., Wang, L., Hou, Y., Ouyang, H., et al. (2015). Dietary Modulation of Gut Microbiota Contributes to Alleviation of Both Genetic and Simple Obesity in Children. EBioMedicine *2*, 968–984. https://doi.org/10.1016/j.ebiom.2015.07.007.

28. Sanchez-Gorostiaga, A., Bajić, D., Osborne, M.L., Poyatos, J.F., and Sanchez, A. (2019). High-order interactions distort the functional landscape of microbial consortia. PLoS Biol. *17*, e3000550. https://doi.org/10.1371/journal.pbio.3000550.

29. Clark, R.L., Connors, B.M., Stevenson, D.M., Hromada, S.E., Hamilton, J.J., Amador-Noguez, D., and Venturelli, O.S. (2021). Design of synthetic human gut microbiome assembly and butyrate production. Nat. Commun. *12*, 3254. https://doi.org/10.1038/s41467-021-22938-y.

30. Wu, G., Xu, T., Zhao, N., Lam, Y.Y., Ding, X., Wei, D., Fan, J., Shi, Y., Li, X., Li, M., et al. (2022). Two Competing Guilds as a Core Microbiome Signature for Health Recovery. Preprint at bioRxiv. https://doi.org/10.1101/2022.05.02.490290.

31. Derosa, L., Routy, B., Thomas, A.M., Iebba, V., Zalcman, G., Friard, S., Mazieres, J., Audigier-Valette, C., Moro-Sibilot, D., Goldwasser, F., et al. (2022). Intestinal Akkermansia muciniphila predicts clinical response to PD-1 blockade in patients with advanced non-small-cell lung cancer. Nat. Med. *28*, 315–324. https://doi.org/10.1038/s41591-021-01655-5.

32. Tsay, J.-C.J., Wu, B.G., Sulaiman, I., Gershner, K., Schluger, R., Li, Y., Yie, T.-A., Meyn, P., Olsen, E., Perez, L., et al. (2021). Lower airway dysbiosis affects lung cancer progression. Cancer Discov *11*, 293–307. https://doi.org/10.1158/2159-8290.CD-20-0263.

33. Chang, C.-C., and Lin, C.-J. (2011). LIBSVM: A library for support vector machines. ACM Trans. Intell. Syst. Technol. *2*, 1–27. https://doi.org/10.1145/1961189.1961199.

34. Messaoudene, M., Pidgeon, R., Richard, C., Ponce, M., Diop, K., Benlaifaoui, M., Nolin-Lapalme, A., Cauchois, F., Malo, J., Belkaid, W., et al. (2022). A Natural Polyphenol Exerts Antitumor Activity and Circumvents Anti-PD-1 Resistance through Effects on the Gut Microbiota. Cancer Discov. *12*, 1070–1087. https://doi.org/10.1158/2159-8290.CD-21-0808.

35. Antoniotti, C., Rossini, D., Pietrantonio, F., Salvatore, L., Marmorino, F., Ambrosini, M., Lonardi, S., Bensi, M., Moretto, R., Tamberi, S., et al. (2023). FOLFOXIRI plus bevacizumab and atezolizumab as upfront treatment of unresectable metastatic colorectal cancer (mCRC): Updated and overall survival results of the phase II randomized AtezoTRIBE study. JCO *41*, 3500. https://doi.org/10.1200/JCO.2023.41.16_suppl.3500.

36. Ma, S., Shungin, D., Mallick, H., Schirmer, M., Nguyen, L.H., Kolde, R., Franzosa, E., Vlamakis, H., Xavier, R., and Huttenhower, C. (2022). Population structure discovery in meta-analyzed microbial communities and inflammatory bowel disease using MMUPHin. Genome Biol *23*, 208. https://doi.org/10.1186/s13059-022-02753-4.

37. Antoniotti, C., Rossini, D., Pietrantonio, F., Catteau, A., Salvatore, L., Lonardi, S., Boquet, I., Tamberi, S., Marmorino, F., Moretto, R., et al. (2022). Upfront FOLFOXIRI plus bevacizumab with or without atezolizumab in the treatment of patients with metastatic colorectal cancer (AtezoTRIBE): a multicentre, open-label, randomised, controlled, phase 2 trial. Lancet Oncol. *23*, 876–887. https://doi.org/10.1016/S1470-2045(22)00274-1.

38. Gharaibeh, R.Z., and Jobin, C. (2019). Microbiota and cancer immunotherapy: in search of microbial signals. Gut *68*, 385–388. https://doi.org/10.1136/gutjnl-2018-317220.

39. Limeta, A., Ji, B., Levin, M., Gatto, F., and Nielsen, J. (2020). Meta-analysis of the gut microbiota in predicting response to cancer immunotherapy in metastatic melanoma. JCI Insight *5*, e140940. https://doi.org/10.1172/jci.insight.140940.

40. Shaikh, F.Y., White, J.R., Gills, J.J., Hakozaki, T., Richard, C., Routy, B., Okuma, Y., Usyk, M., Pandey, A., Weber, J.S., et al. (2021). A Uniform Computational Approach Improved on Existing Pipelines to Reveal Microbiome Biomarkers of Nonresponse to Immune Checkpoint Inhibitors. Clin. Cancer Res. *27*, 2571–2583. https://doi.org/10.1158/1078-0432.CCR-20-4834.

41. Cortellini, A., Tucci, M., Adamo, V., Stucci, L.S., Russo, A., Tanda, E.T., Spagnolo, F., Rastelli, F., Bisonni, R., Santini, D., et al. (2020). Integrated analysis of concomitant medications and oncological outcomes from PD-1/PD-L1 checkpoint inhibitors in clinical practice. J. Immunother. Cancer *8*, e001361. https://doi.org/10.1136/jitc-2020-001361.

42. Imhann, F., Bonder, M.J., Vich Vila, A., Fu, J., Mujagic, Z., Vork, L., Tigchelaar, E.F., Jankipersadsing, S.A., Cenit, M.C., Harmsen, H.J.M., et al. (2016). Proton pump inhibitors affect the gut microbiome. Gut *65*, 740–748. https://doi.org/10.1136/gutjnl-2015-310376.

43. Jackson, M.A., Verdi, S., Maxan, M.-E., Shin, C.M., Zierer, J., Bowyer, R.C.E., Martin, T., Williams, F.M.K., Menni, C., Bell, J.T., et al. (2018). Gut microbiota associations with common diseases and prescription medications in a population-based cohort. Nat. Commun. *9*, 2655. https://doi.org/10.1038/s41467-018-05184-7.

44. Cosseau, C., Devine, D.A., Dullaghan, E., Gardy, J.L., Chikatamarla, A., Gellatly, S., Yu, L.L., Pistolic, J., Falsafi, R., Tagg, J., and Hancock, R.E. (2008). The commensal Streptococcus salivarius K12 downregulates the innate immune responses of human epithelial cells and promotes host-microbe homeostasis. Infect. Immun. *76*, 4163–4175. https://doi.org/10.1128/IAI.00188-08.

45. Bernardo, D., Sánchez, B., Al-Hassi, H.O., Mann, E.R., Urdaci, M.C., Knight, S.C., and Margolles, A. (2012). Microbiota/Host Crosstalk Biomarkers: Regulatory Response of Human Intestinal Dendritic Cells Exposed to Lactobacillus Extracellular Encrypted Peptide. PLOS ONE *7*, e36262. https://doi.org/10.1371/journal.pone.0036262.

46. Santos Rocha, C., Lakhdari, O., Blottière, H.M., Blugeon, S., Sokol, H., Bermúdez-Humarán, L.G., Azevedo, V., Miyoshi, A., Doré, J., Langella, P., et al. (2012). Anti-inflammatory properties of dairy lactobacilli. Inflamm. Bowel Dis. *18*, 657–666. https://doi.org/10.1002/ibd.21834.

47. Ghosh, T.S., Das, M., Jeffery, I.B., and O'Toole, P.W. (2020). Adjusting for age improves identification of gut microbiome alterations in multiple diseases. eLife *9*, e50240. https://doi.org/10.7554/eLife.50240.

48. Stanley, D., Mason, L.J., Mackin, K.E., Srikhanta, Y.N., Lyras, D., Prakash, M.D., Nurgali, K., Venegas, A., Hill, M.D., Moore, R.J., and Wong, C.H. (2016). Translocation and dissemination of commensal bacteria in post-stroke infection. Nat. Med. *22*, 1277–1284. https://doi.org/10.1038/nm.4194.

49. Gupta, V.K., Kim, M., Bakshi, U., Cunningham, K.Y., Davis, J.M., Lazaridis, K.N., Nelson, H., Chia, N., and Sung, J. (2020). A predictive index for health status using species-level gut microbiome profiling. Nat. Commun. *11*, 4635. https://doi.org/10.1038/s41467-020-18476-8.

50. Frankel, A.E., Coughlin, L.A., Kim, J., Froehlich, T.W., Xie, Y., Frenkel, E.P., and Koh, A.Y. (2017). Metagenomic Shotgun Sequencing and Unbiased Metabolomic Profiling Identify Specific Human Gut Microbiota and Metabolites Associated with Immune Checkpoint Therapy Efficacy in Melanoma Patients. Neoplasia *19*, 848–855. https://doi.org/10.1016/j.neo.2017.08.004.

51. Chaput, N., Lepage, P., Coutzac, C., Soularue, E., Le Roux, K., Monot, C., Boselli, L., Routier, E., Cassard, L., Collins, M., et al. (2017). Baseline gut

microbiota predicts clinical response and colitis in metastatic melanoma patients treated with ipilimumab. Ann. Oncol. *28*, 1368–1379. https://doi.org/10.1093/annonc/mdx108.

52. Danlos, F.-X., Grajeda-Iglesias, C., Durand, S., Sauvat, A., Roumier, M., Cantin, D., Colomba, E., Rohmer, J., Pommeret, F., Baciarello, G., et al. (2021). Metabolomic analyses of COVID-19 patients unravel stage-dependent and prognostic biomarkers. Cell Death Dis. *12*, 258. https://doi.org/10.1038/s41419-021-03540-y.
53. Peyraud, F., Guégan, J.P., Bodet, D., Nafia, I., Fontan, L., Auzanneau, C., Cousin, S., Roubaud, G., Cabart, M., Chomy, F., et al. (2022). Circulating L-arginine predicts the survival of cancer patients treated with immune checkpoint inhibitors. Ann. Oncol. *33*, 1041–1051. https://doi.org/10.1016/j.annonc.2022.07.001.
54. Geiger, R., Rieckmann, J.C., Wolf, T., Basso, C., Feng, Y., Fuhrer, T., Kogadeeva, M., Picotti, P., Meissner, F., Mann, M., et al. (2016). L-Arginine Modulates T Cell Metabolism and Enhances Survival and Anti-tumor Activity. Cell *167*, 829–842.e13. https://doi.org/10.1016/j.cell.2016.09.031.
55. Canale, F.P., Basso, C., Antonini, G., Perotti, M., Li, N., Sokolovska, A., Neumann, J., James, M.J., Geiger, S., Jin, W., et al. (2021). Metabolic modulation of tumours with engineered bacteria for immunotherapy. Nature *598*, 662–666. https://doi.org/10.1038/s41586-021-04003-2.
56. Teng, H., Wang, Y., Sui, X., Fan, J., Li, S., Lei, X., Shi, C., Sun, W., Song, M., Wang, H., et al. (2023). Gut microbiota-mediated nucleotide synthesis attenuates the response to neoadjuvant chemoradiotherapy in rectal cancer. Cancer Cell *41*, 124–138.e6. https://doi.org/10.1016/j.ccell.2022.11.013.
57. Wirbel, J., Zych, K., Essex, M., Karcher, N., Kartal, E., Salazar, G., Bork, P., Sunagawa, S., and Zeller, G. (2021). Microbiome meta-analysis and cross-disease comparison enabled by the SIAMCAT machine learning toolbox. Genome Biol. *22*, 93. https://doi.org/10.1186/s13059-021-02306-1.
58. Sonpavde, G.P., Sternberg, C.N., Loriot, Y., Marabelle, A., Lee, J.L., Fléchon, A., Roubaud, G., Pouessel, D., Zagonel, V., Calabro, F., et al. (2022). Primary results of STRONG: An open-label, multicenter, phase 3b study of fixed-dose durvalumab monotherapy in previously treated patients with urinary tract carcinoma. Eur. J. Cancer *163*, 55–65. https://doi.org/10.1016/j.ejca.2021.12.012.
59. Jacomy, M., Venturini, T., Heymann, S., and Bastian, M. (2014). ForceAtlas2, a Continuous Graph Layout Algorithm for Handy Network Visualization Designed for the Gephi Software. PLOS ONE *9*, e98679. https://doi.org/10.1371/journal.pone.0098679.
60. Beghini, F., McIver, L.J., Blanco-Míguez, A., Dubois, L., Asnicar, F., Maharjan, S., Mailyan, A., Thomas, A.M., Manghi, P., Valles-Colomer, M., et al. (2021). Integrating taxonomic, functional, and strain-level profiling of diverse microbial communities with bioBakery. Elife *10*, e65088. https://doi.org/10.7554/eLife.65088.

STAR★METHODS

KEY RESOURCES TABLE

REAGENT or RESOURCE	SOURCE	IDENTIFIER
Deposited data		
Raw data	This paper	BioProject PRJNA1023797
Software and algorithms		
Python version 3.7.11	Python Software Foundation	https://www.python.org
MetaPhlAn 4.0	The Huttenhower Lab	https://huttenhower.sph.harvard.edu/metaphlan/
HUMAnN 3.0	The Huttenhower Lab	https://huttenhower.sph.harvard.edu/humann
Pandas 1.3.4	Python Software Foundation	https://pypi.org/project/pandas/
R 4.2.2	The R Foundation for Statistical Computing	https://www.r-project.org/
R survival package 3.5-7	CRAN R Project	https://cran.r-project.org/package=survival
SIAMCAT R package 2.6.0	Wirbel et al.[57]	https://doi.org/10.18129/B9.bioc.SIAMCAT
Dask v2021.10.0	Python Software Foundation	https://docs.dask.org/en/stable/
Other		
Tabular patients' data used for analysis, clinical metadata, healthy-volunteers data and metadata, Toposcore main and helper R scripts	This paper	https://github.com/valerioiebba/TOPOSCORE

RESOURCE AVAILABILITY

Lead contact

Further information and requests for resources and reagents should be directed to and will be fulfilled by the lead contact, Docteur Lisa Derosa (lisa.derosa@gutaveroussy.fr), and corresponding author, Professor Laurence Zitvogel (laurence.zitvogel@gustaveroussy.fr).

Materials availability

This study did not generate new unique reagents.

Data and code availability

- The data generated or analyzed during this study are included within the paper, its supplemental information files and public repositories. Raw metagenomic sequences data and metadata derived from human feces samples ($n = 499$) have been deposited at NCBI SRA database under the Bioproject PRJNA1023797 and are publicly available as of the date of publication. Accession numbers are listed in the key resources table. This paper analyzes existing, publicly available data and metadata (for healthy volunteers: https://doi.org/10.1038/nmeth.4468; for melanoma: https://doi.org/10.1038/s41591-022-01695-5; for colorectal cancer (CRC): https://ascopubs.org/doi/10.1200/JCO.2023.41.16_suppl.3500). The key resources table reports raw data produced in the present article, along with patients' metadata and raw data (GitHub repository).
- The entire analysis for TOPOSCORE calculation was programmed in *R* (see key resources table) All original code is available in supplemental information of the paper and at the GitHub repository (https://github.com/valerioiebba/TOPOSCORE).
- Any additional information required to reanalyze the data reported in this paper is available from the lead contact upon request.

STUDY PARTICIPANT DETAILS

Patient cohorts and specimen

All data and sample collection and all clinical trials were performed in compliance with regulatory, ethical, and European GDPR requirements. The written informed consent was obtained for all patients in accordance with the World Medical Association (WMA)'s

Declaration of Helsinki as revised in 2013. Feces collection for metagenomics analysis were performed under the study ONCOBIOTICS* (Sponsor Protocol N: CSET 2017/2619, ID-RCB N: 2017-A02010-53) according to the ethical guidelines and approval of the local ethical committee (Comité Consultatif de Protection des Personnes dans la Recherche Biomédicale (CCPPRB) of the Kremlin Bicêtre Hospital). Sex-related data (sex assigned at birth) and information about age (in years, from inclusion in protocol) are provided here for all study participants. Ancestry, race, ethnicity, socioeconomic status are not provided here for all study participants due to France's Data Protection Act No. 78-17 created the French Data Protection Authority (Commission Nationale Informatique et Libertés [CNIL]). Article 8 of this legislation states: 'The collection and processing of personal data that reveals, directly or indirectly, the racial and ethnic origins, the political, philosophical, religious opinions or trade union affiliation of persons, or which concerns their health or sexual life, is prohibited'.[https://www.advamed.org/sites/default/files/resource/112_112_code_of_ethics_0.pdf]

General Data Protection Regulation procedures and anonymization rules have been applied according to Oncobiome H2020 model system already in place in the ClinicObiome, Gustave Roussy. The bladder cancer cohort of patients allowing the IOPREDI / STRONG ancillary study biobanking and data mining was provided by AstraZeneca. IOPREDI (EudraCT Number: 2016-005068-33) is the French cohort of the STRONG phase IIIb trial.[58] The Clinical Study Protocols and Informed Consent Forms were approved by Independent Ethics Committees/Institutional Review Boards.[58] Patients with bladder cancer who progressed on previous chemotherapy were treated with durvalumab (1500 mg every 4 weeks until progression). Baseline stool samples were used for MG analyses (n=133) and pooled with the kidney cancer cohort from ONCOBIOTICS.

The melanoma patient cohort (PRIMM-UK) was analyzed and reported by University of Trento (Dr N. Segata).

The colorectal cancer (CRC) cohort from the AtezoTRIBE study provided stool biobanking and data mining (GONO foundation).[35,37] AtezoTRIBE was a prospective phase II clinical trial, which enrolled 218 patients affected by unresectable Stage IV CRC to receive two first line systemic regimens. These patients were not subjected to any other treatment at the time of the first stool sample collection. In particular, 150 stool samples were available for the first time point for the same number of patients, considering only MSS CRC treated with chemoimmunotherapy. Samples were collected using the same guidelines and processes as for the ONCOBIOTICS cohorts.

METHOD DETAILS

Shotgun metagenomics sequencing and bioinformatic analysis

For metagenomic analysis, the stools were processed for total DNA extraction and sequencing with Ion Proton technology following MetaGenoPolis (INRAE) France, as previously reported. Metagenomic analysis of fastq files was performed following previously published guidelines[7] for taxonomic (MetaPhlAn 4.0) and functional (HUMAnN 3.0)[59] profiling of metagenomes. These two pipelines leverage a set of 99,200 high-quality and fully annotated reference microbial genomes spanning 16,800 species and the 87.3 million UniRef90 functional annotations available in UniProt. The taxonomic profiling and quantification of organisms' relative abundances of all metagenomic samples were quantified using MetaPhlAn 4.0 with default parameters. In total, we identified 536 microbial species. *Statistical analysis for* Figure S1. For the forthcoming statistical and metagenomic analysis, patients were randomly distributed into a discovery cohort (n=245) and validation cohort (n=254) by means of the Python ''pandas'' package v1.3.4, ''df.sample'' function. Overall survival (OS), defined as the time from immune checkpoint inhibitor treatment start until death from any cause, was estimated using the Kaplan–Meier method and compared with the log-rank test (Mantel–Cox method) in a univariate analysis. Multivariate survival analyses were performed using Cox regression models to determine hazard ratios and 95% confidence intervals for overall survival adjusting for variables with p-values < 0.05 found in univariate analysis using the coxph function from the R *survival* package (v3.2-7). Survival analysis and Kaplan-Meier curves were computed (R v4.1.2 packages survival, survminer, Rcpp) for each microbial species harbored by each of the seven SIGs, retrieving survival curves parameters as per survfit function (records, n.max, n.start, events, rmean, se_rmean, median, 0.95LCL, 0.95UCL) and per survdiff function (Observed, Expected, (O-E)^2/E, (O-E)^2/V, Chi-squared, P value) (Supplementary Table KM_calculations). These parameters were computed using the ''high'' and ''low'' relative abundances (considering the ''high''≥ 0 and the ''low''<0 of normalized and standardized relative abundance values as cut-off values). We then computed the difference (ΔHigh-Low mOS) and fold-ratio (log2FRHigh/Low mOS) in median OS for each microbial species, finding out a hierarchy of positive to negative microbial species in terms of their contribution to patients' mOS.

Statistical analysis of metagenomic data

Within data matrices retrieved from the MetaPhlAn 4.0 pipeline, only microbial species having a prevalence $\geq 2.5\%$ were considered for subsequent analysis. Relative abundances of microbial species underwent transformation (multiplicative_replacement followed by centre-log-ratio clr functions, Sci-Kit learn package v1.0.1), then normalization and standardization using QuantileTransformer and StandardScaler methods from Sci-Kit learn package v1.0.1. Normalization using the output_distribution='normal' option transforms the distribution of each variable to a Gaussian-like, while the standardization results in each normalized variable distribution having a mean of zero and unit variance. These two steps of normalization and standardization ensure the proper comparison of variables with different dynamic ranges, such as microbial relative abundances. Data were batch-corrected with MMUPHin (Ma et al. 2022).[36] For microbiota analysis, measurements of α diversity (within sample diversity) such as Richness and Shannon index, were calculated at species level using the SciKit-bio package v0.5.6. Exploratory analysis of β-diversity (between sample diversity)

was calculated using the 'Bray-Curtis' measure of dissimilarity and 'complete linkage' method, and represented in Principal Coordinate Analyses (PCoA) as an ordination plot. Metrics to compare groups of multivariate sample units (analysis of similarities - ANOSIM, permutational multivariate analysis of variance - PERMANOVA) were employed to assess significance in data points clustering.[39] ANOSIM and PERMANOVA were automatically calculated after 999 permutations, as implemented in SciKit-bio package v0.5.6. We implemented Partial Least Square Discriminant Analysis (PLS-DA) and the subsequent Variable Importance Plot (VIP) as a supervised analysis wherein the VIP values (order of magnitude) are used to identify the most discriminant microbial species among the cohorts. Bar thickness reports the fold ratio (FR) value of the mean relative abundances for each species among the two cohorts, while an absent border indicates mean relative abundance of zero in the compared cohort. Mann-Whitney U test and Kruskal-Wallis tests were employed to assess significance for pairwise or multiple comparisons, respectively, considering a P value $\leq$0.05 as significant. All P values were corrected for multiple hypothesis testing using a two-stage Benjamini-Hochberg FDR at 10%. Receiver Operating Characteristic (ROC) metric to evaluate classifier output quality was generated by a machine learning model employed in Sci-Kit learn package v1.0.1 trained on ICI response, using the ML standard in metagenomics, a random forest classifier within Sci-Kit learn package v1.0.1. Classifier parameters were: L1 regularization, n_estimators=1000, class_weight='balanced_subsample', random_state=0, oob_score=True, n_jobs=-1, max_depth=2, bootstrap=True, criterion='gini'. Venn diagrams were generated from selected species using the online software InteractiVenn, available at http://www.interactivenn.net/. All the analyses were made with Python v3.8.2 or R v4.1.2. Sankey diagram was generated with the Plotly library within Python v3.8.2.

Toposcore algorithm

The scoring algorithm was developed based on the relative abundance of 536 metagenomics species (MGS) derived from 245 NSCLC cancer patients of the discovery cohort (Table S1).

Each MGS was categorized as "low" or "high" if its relative abundance $\leq$ or >median respectively. When a MGS had a majority of null abundances (i.e., median = 0), this process matched the "absence" vs "presence" categorization. Cox Proportional Hazard (CoxPH) models were run on "overall survival" for each categorized MGS. A total of 266 MGS with a Hazard Ratio (HR) $\leq$ 0.80 or $\geq$ 1.25 were retained in the model. The purpose of this selection was to discard MGS with HR close to 1, which are unlikely to participate in a diagnostic signature. Selected MGS were not necessarily significantly associated with OS as 1 might be contained in the 95% Confidence Interval (CI) of their HR. The *Akkermansia muciniphila* MGS was not considered in this screening because its relative abundance had a trichotomic distribution with no linear dose-effect relationship with patient prognosis as already reported in details.[31] Each pair of MGS was then analyzed by a Fisher's exact test on 2x2 contingency tables based on their Absence/Presence co-occurrences and scored by the $-\log_{10}(p)$ x sign (OR – 1) metrics, where p is the Fisher p-value and OR the Odds Ratio of the 2x2 table. This metrics defined a score proportional to the significance of the interaction between two MGS ($-\log_{10}(p)$) that is negative in case of co-exclusion pattern (OR < 1) or positive in case of co-occurrence (OR > 1). Interactions with a Bonferroni-corrected p-value $\leq$ 0.05 were retained for analysis. A total of 180 connected MGS were then clustered with Ward's method and Manhattan distance. The clustering tree was cut to obtain 7 clusters (C1 to C7). Two clusters (C5 and C6) contained 37 MGS mostly (95%) associated with OS<12 (HR $\geq$ 1.25) that were used to define the SIG1 signature. Three clusters (C1, C2, C3) contained 45 MGS all associated with OS>12 months (HR $\leq$ 0.80) that were used to define the SIG2 signature. In addition, interactions within SIG1 and SIG2 MGS were 99% and 100% positive respectively (co-occurrence patterns), while edges in-between SIG1 and SIG2 MGS were 98% negative (co-exclusion patterns), thus reflecting a significant and opposite topological separation.

Each patient of the discovery cohort was then scored with a S score computed as the difference of proportions between present (relative abundance > 0) SIG2 and SIG1 MGS and scaled from 0 to 1: S = (#SIG2/45 - #SIG1/37 + 1)/2. A score of 0 indicates that all MGS of the SIG1 signature have strictly positive relative abundances and all MGS of the SIG2 signature have null relative abundances. Conversely, a score of 1 indicates that all MGS of the SIG1 signature have null relative abundances and all MGS of the SIG2 signature have strictly positive relative abundances. A score of 0.5 indicates an equilibrium in proportions of present SIG1 and SIG2 MGS. The performance of this S score was analyzed by a Receiver Operating Characteristic (ROC) analysis. Two scores, 0.5351 and 0.7911, were identified as local maxima of the Youden index (Specificity + Specificity – 1) and were used as cutoffs to define three categories: SIG1+ if S $\leq$ 0.5351, SIG2+ if S $\geq$ 0.7911, and "gray zone" otherwise.

The association with OS was made based on these categories: OS<12 in the SIG1+ category, and OS>12 in the SIG2+ category. The gray zone defines a range of scores where the relative proportions of present SIG2 and SIG1 MGS hardly discriminated survival outcomes. In this range, the Gram⁻ anaerobic bacterium *Akkermansia muciniphila* SGB9226, for which a trichotomized distribution of the relative abundance was shown to correlate with OS,[31] was used: OS>12 if *Akkermansia muciniphila* is low (in normal ranges), OS<12 if *Akkermansia muciniphila* is 0 or high (abnormal ranges). The performance was assessed by Kaplan Meier (KM) analyses of predicted OS>12 vs. OS<12 in CoxPH analyses of OS in the discovery cohort, and repeated on several independent cohorts.

Machine learning approach for responsiveness to immunotherapy

First, we trained a RF classifier (SIAMCAT R package 1,000 estimator trees, with a minimumof 30% of features par tree)[57] on the discovery cohort in a 10-fold cross validation repeated 20 times, to assess AUC. Siamcat algorithm was used for the RF model, and its performance was measured by ROC curves and AUC value. Second, the 284 metagenome-assembled genomes (MAGs) from Guild1 and Guild2 found in our previous work were used as reference genomes to perform read recruitment analysis.[30] The

metagenomic reads were aligned to the MAGs using coverM with –min-read-aligned-percent 90 –min-read-percent-identity 99. Abundances of the MAGs were used for the RF model, and its performance was measured by ROC curves and confusion matrix.

Gene Pathway Functional analyses

Functional potential analysis of the metagenomic samples was performed using HUMAnN 3.0[60] with default parameters. The MetaCyc ''path abundance'' profiles, expressed as RPK units, were analyzed by Dask v2021.10.0 (https://docs.dask.org/en/stable/), in order to have a final matrix of pathways, both bulk and species-specific. Subsequent statistical analysis was performed as described in the paragraph ''Statistical analysis of metagenomic data'', taking into consideration only the pathways with a prevalence equal or higher than 20%, and the patients' categorization into SIG1+ and SIG2+ following TOPOSCORE. In order to analyze the different pathways composition among SIG, each SIG species was measured for its contribution to each pathway, and RPK unit results expressed as mean±SEM.

qPCR-based TOPOSCORE using Precision Microbiome Profiling (PMP™)

For each bacterium and archaea, we used the *coords* function of the *pROC* R package to determine the cut-off of qPCR amplification using the Youden index allowing to reproduce the community detection of our reference measurement (shotgun metagenomics) with the best trade-off in terms of sensitivity and specificity. Due to the non-linear relationship between the PCR quantification and the presence status of *Akkermansia* spp. relative abundance (negative if Akk=0 or Akk$\geq$4.8, and positive if 0<Akk<4.8), we considered three categories: negative/low (Akk=0), positive (0<Akk<4.8), and negative/high (Akk$\geq$4.8). We determined two PCR cut-offs according to the Youden index for multinomial response with the multiclass.roc function of the pROC R package. These analyses were realized using R v4.0.4.

ADDITIONAL RESOURCES

Clinical trial registry numbers

- ONCOBIOTICS (https://clinicaltrials.gov/ct2/show/NCT04567446)
- IOPREDI / STRONG ancillary study (https://clinicaltrials.gov/study/NCT03084471)
- PRIMM-UK (https://clinicaltrials.gov/study/NCT03643289)
- AtezoTRIBE (https://clinicaltrials.gov/study/NCT03721653)

CellPress
OPEN ACCESS

Supplemental figures

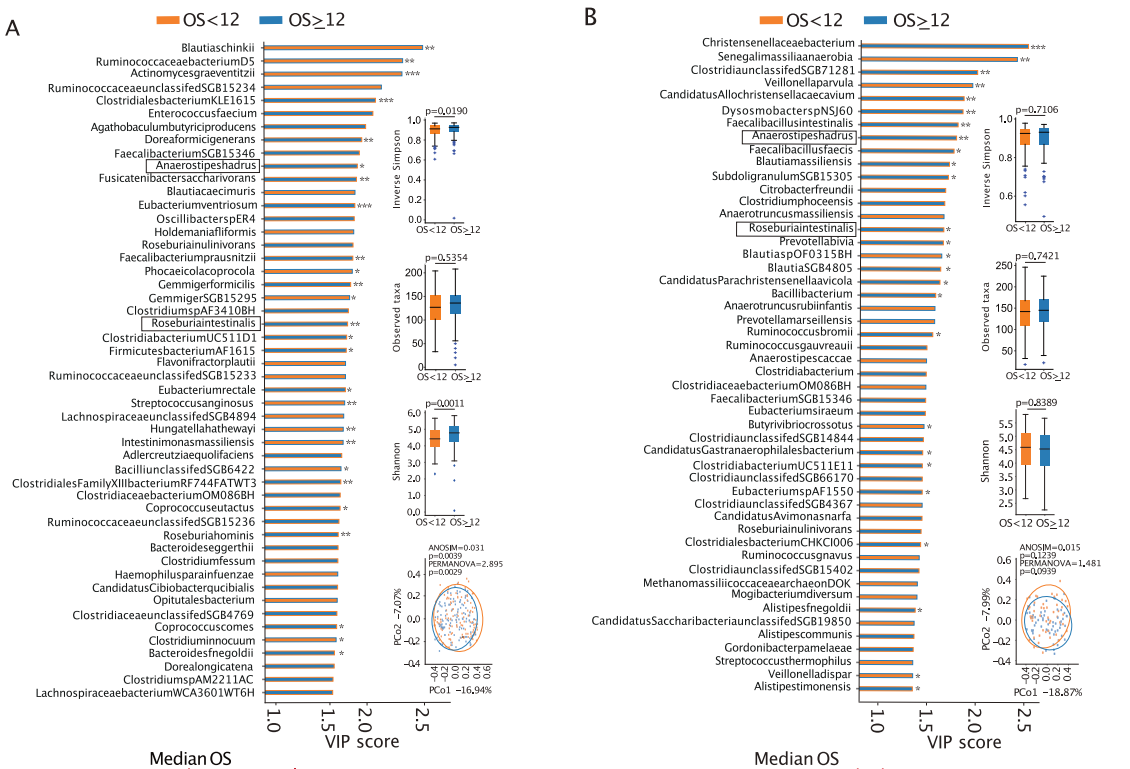

(legend on next page)

Figure S1. Classical method to estimate the performance of MGSs associated with clinical benefit to immune-checkpoint blockade

(A and B) Taxonomic alpha-diversities (insets) of patient samples were estimated using the inverse Simpson index, observed taxa, and Shannon diversity index (right, upper). Alpha-diversity metrics were computed for non-responders (OS < 12 months, orange) and responders (OS ≥12 months, blue) patients with follow up >12 months from the discovery cohort (A) and the validation (B) cohorts. Beta-diversities (principal coordinate analysis, PCoA) of fecal microbiota (microbial relative abundances) according to response (orange: OS < 12 months, blue: OS ≥ 12 months.) in the discovery cohort (A) and the validation (B) cohorts (right, lower). Supervised analysis using partial least square discriminant analysis (PLS-DA) and variable importance plot (VIP) to identify the most discriminant microbial species among non-responders (OS < 12 months, orange) and responders (OS ≥ 12 months, blue) (left). ANOSIM and PERMANOVA define the separation of the groups; *p* values define the significance of group separation after 999 permutations of the samples. Mann-Whitney U test *p* values (*$p < 0.05$, **$p < 0.01$, ***$p < 0.001$) are indicated.

(C–F) Cox regression univariate analysis and Kaplan-Meier curves of OS of NSCLC patients in discovery (C and D) and validation (E and F) cohorts according to the presence or absence of *Roseburia intestinalis* (C and E) or *Anaerostipes hadrus* (D and F) in stools at baseline (left). The prevalence of each bacterium is detailed in the right panels. Chi-square test was employed to assess differences in prevalence values.

(G) Receiver operating characteristic (ROC) curves and AUC measuring the performance of the relative abundance of most significant MGSs retained in machine-learning algorithms using the discovery and validation cohorts.

(H) Cox regression univariate analysis and Kaplan-Meier curves of OS in patients with renal cell carcinoma (RCC). All analyses were performed using the MetaPhlAn 4.0 pipeline. Refer to Table S1 for patient characteristics. OS, overall survival; HR, hazard ratio; AUC, area under the ROC curve.

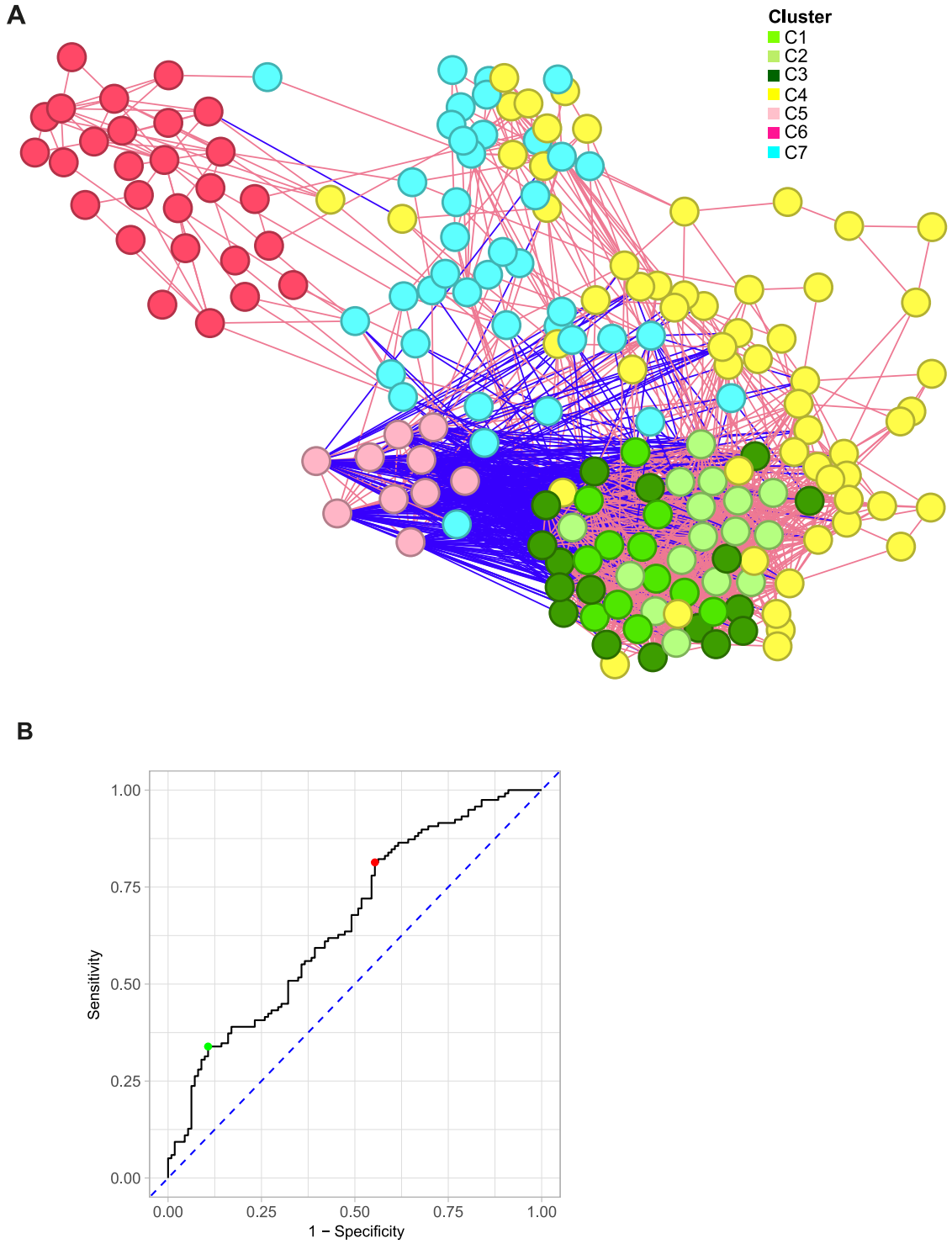

Figure S2. Co-abundance networks and SIGs associated with overall survival in the discovery cohort of patients with NSCLC

(A) Microbial network of the discovery cohort ($n = 245$) using co-occurrence matrices of 180 selected metagenomics species (MGSs). Edges are significant ($p \leq 0.001$) Fisher associations (pink and blue lines for co-occurrence and co-exclusion patterns, respectively). Nodes (representing MGSs) were colored according to the 7 identified co-occurrence clusters, C1 to C7 (refer to Figure S3).

(B) The performance of the S score and its association with OS at 12 months (OS12) was analyzed by a receiver operating characteristic (ROC) analysis. Two scores, 0.5351 and 0.7911, were identified as local maxima of the Youden index (indicated by red and green dots, respectively).

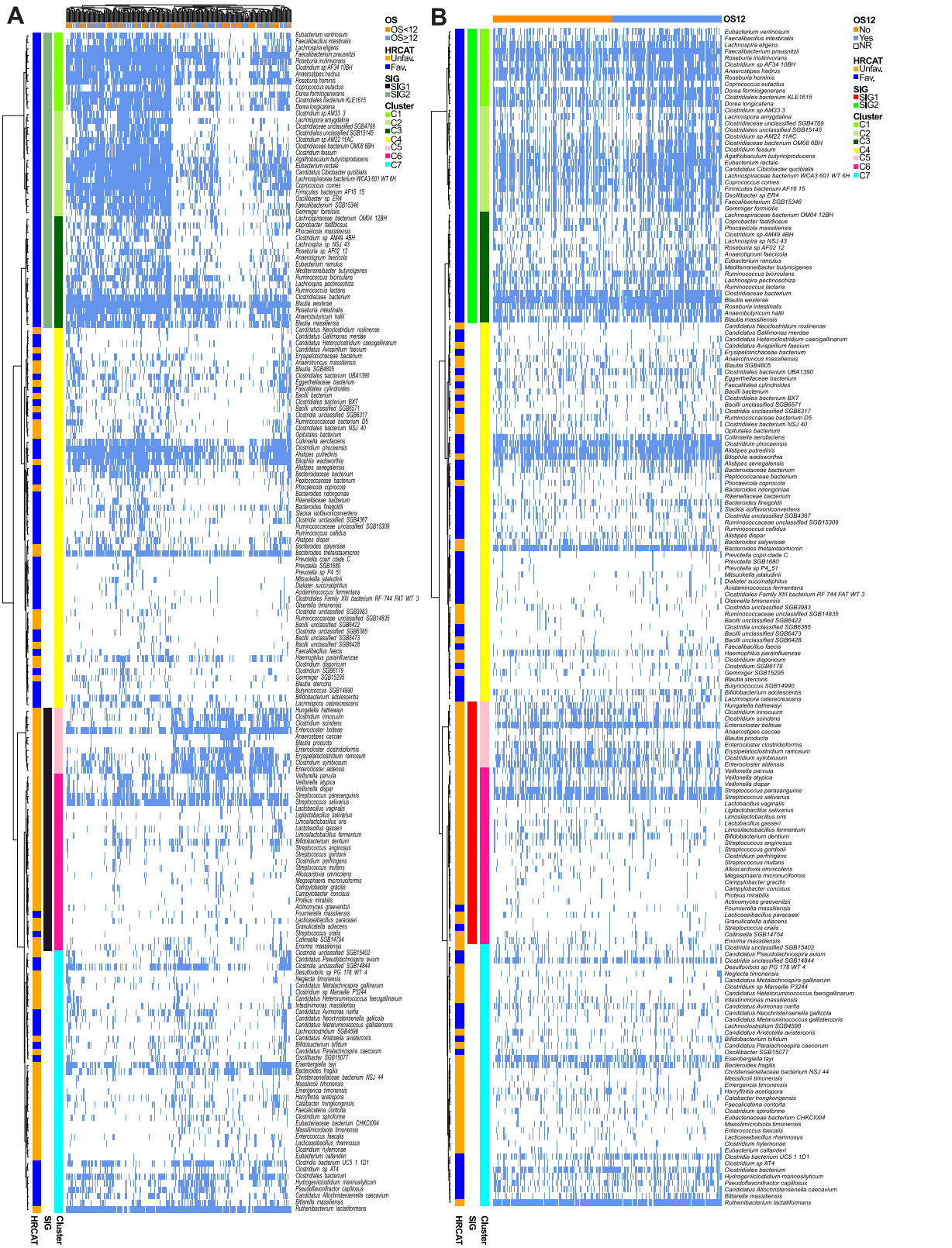

(legend on next page)

Figure S3. Unsupervised hierarchical clustering of the bacteria associated with overall survival retained in the model in the discovery cohort

(A) A total of 180 metagenomics species (MGSs) were clustered with Ward's method and Manhattan distance based on their presence in the discovery cohort (n = 245). In this heatmap, MGSs are in rows and subjects in columns. Presence of a given MGS in a subject is indicated in light blue (and absence in white). On the top scale, the OS status of patients at 12 months is indicated (blue for OS $\geq$ 12 months, orange for OS < 12 months, white for subjects with follow up < 12 months). Seven MGS clusters, C1 to C7, were identified. Clusters C1 to C3 contained MGSs uniquely associated with favorable OS outcome (HR $\leq$ 0.80, in dark blue in the scale on the left) and were assigned to SIG2 group (green). Clusters C5 and C6 contained MGSs mostly associated with unfavorable OS outcome (HR $\geq$ 1.25, in orange) and were assigned to SIG1 group (pink and red). HR, hazard ratio.

(B) Idem as in (A), but the clustering was supervised based on OS12.

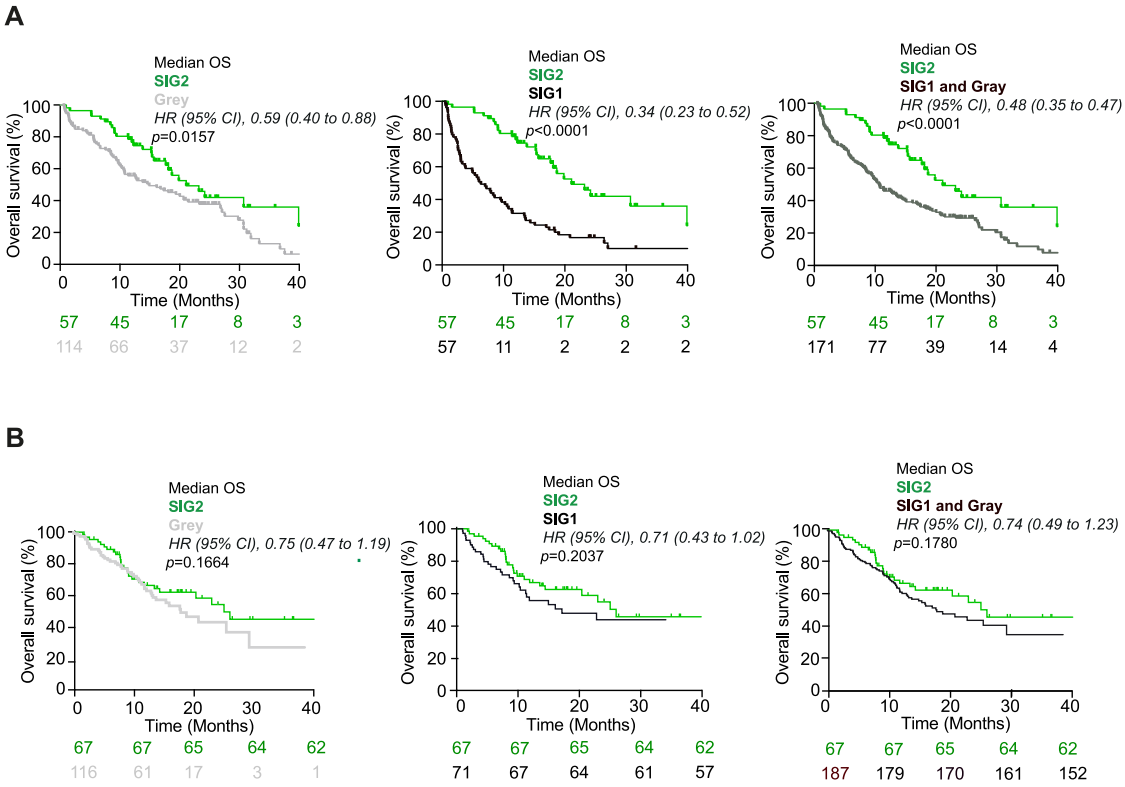

Figure S4. Performance of the S score in the discovery and validation cohorts

(A) Cox regression univariate analysis and Kaplan-Meier curves of overall survival (OS) for the 245 NSCLC patients from the discovery cohort according to the 3 regions within the S score: (1) a SIG1 region ($0 < x < 0.535$); (2) a gray zone ($0.535 \leq x < 0.791$); (3) a SIG2 region ($x \geq 0.791$) calculated from MG of fecal samples at baseline.

(B) Idem as in (A), but for the 254 NSCLC patients from the validation cohort. Cox's proportional-hazards analysis and log rank tests were applied for all Kaplan-Meier curves.

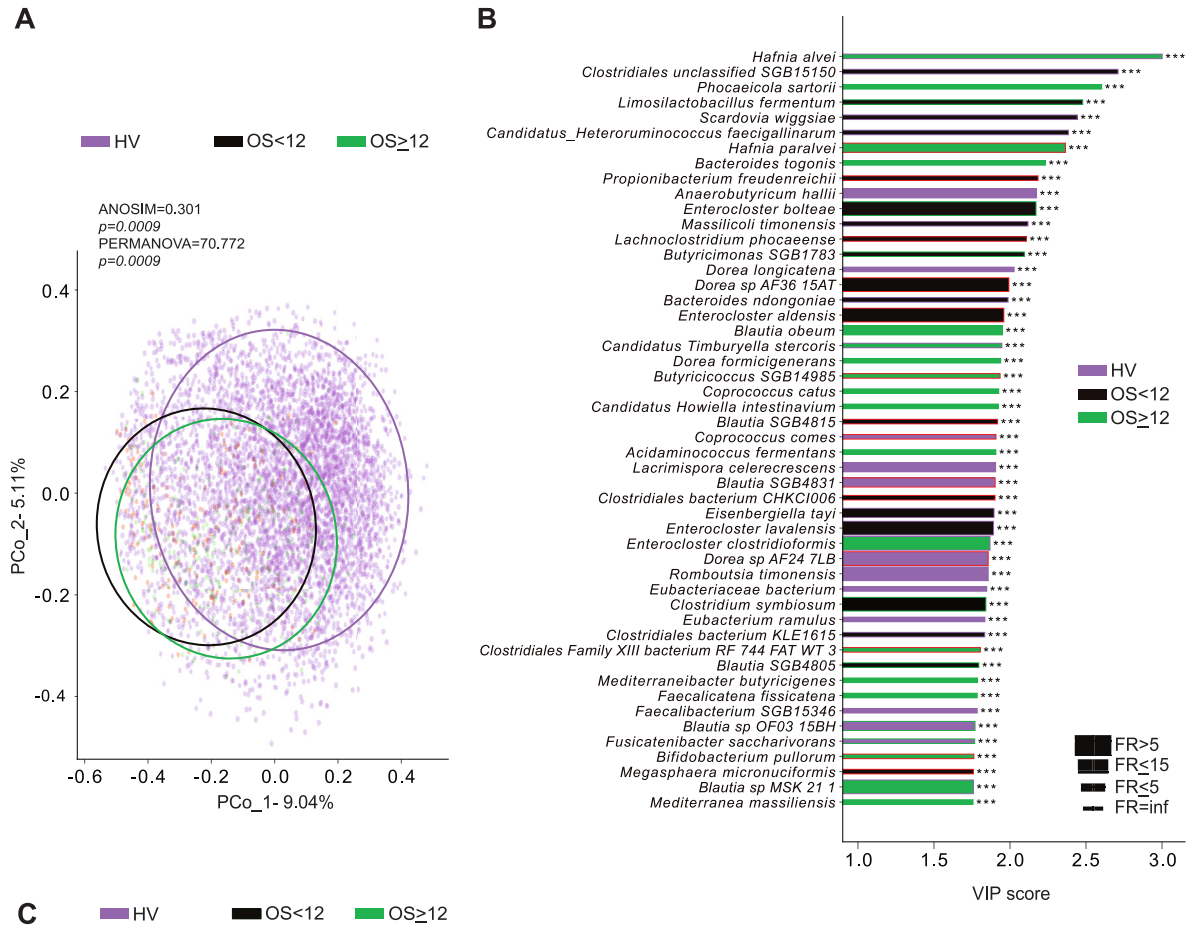

(legend on next page)

Figure S5. TOPOSCORE calculation in healthy volunteers and comparisons with cancer patients classified according to overall survival at 12 months

(A) Beta-diversity (principal coordinate analysis, PCoA) of fecal microbiota (microbial relative abundance) according to individual subgroups: patients with non-small cell lung cancer (NSCLC) and renal cell carcinoma (RCC) and OS < 12 months (black), patients with NSCLC/RCC and OS > 12 months (green), and healthy volunteers (HV) matched on age and geography with cancer patients (purple).

(B) We implemented partial least square discriminant analysis (PLS-DA) and the subsequent variable importance plot (VIP) as a supervised analysis in order to identify the most discriminant microbial species among the patient (OS< or >12) and HV groups. ANOSIM and PERMANOVA define the separation of the groups; *p* values define the significance of group separation after 999 permutations of the samples. Mann-Whitney U test *p* values (*$p < 0.05$, **$p < 0.01$,***$p < 0.001$) are indicated.

(C) SIG1 and SIG2 ratio distributions for all patients with NSCLC and HV are depicted.

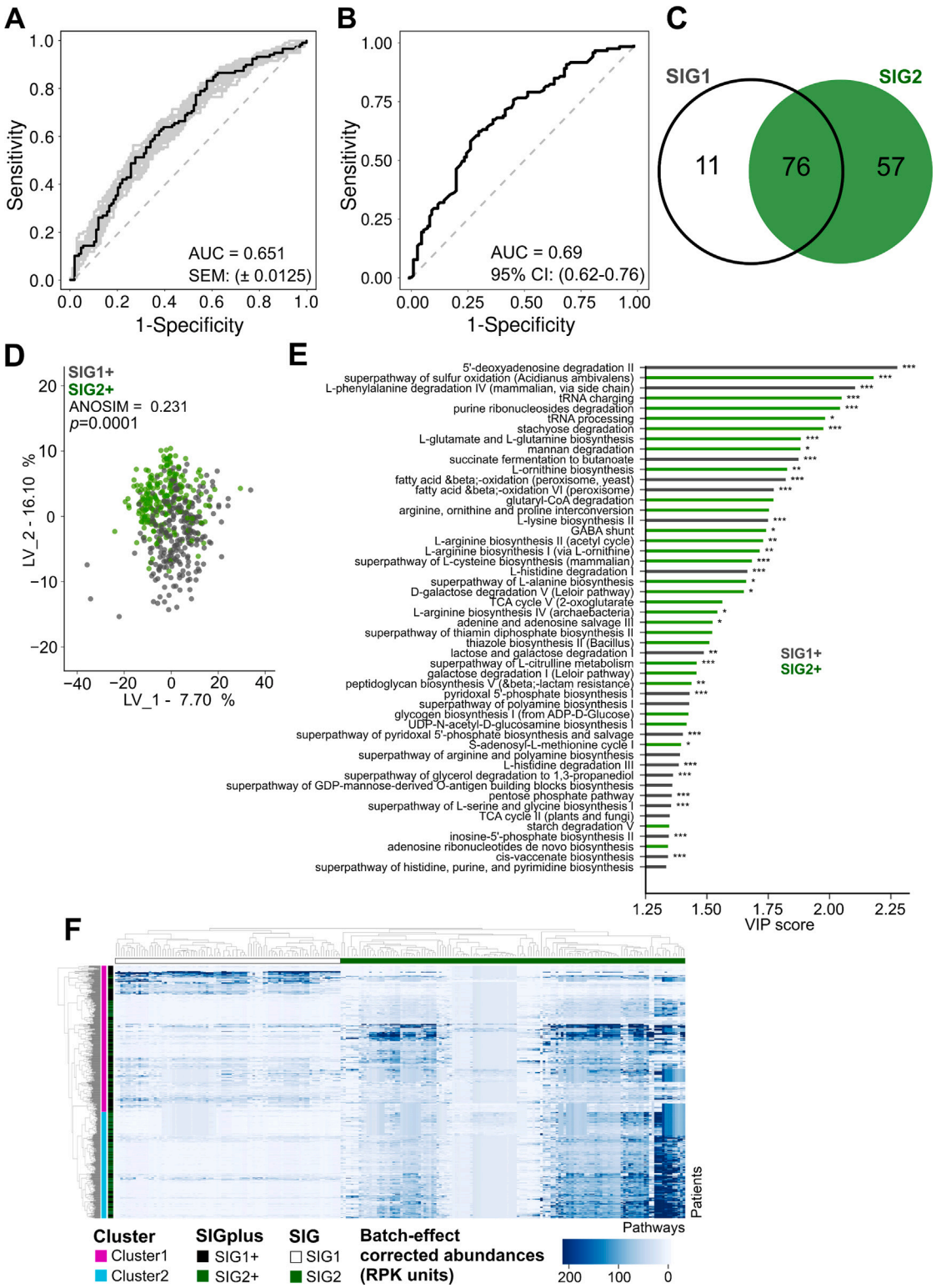

Figure S6. Machine-learning algorithms based on RF or HQ-MAGs and SIG-related functional pathways

(A and B) *Machine-learning algorithms* using random forest (RF) classifier trained on the discovery cohort. SIAMCAT algorithm (A) and abundances of 284 high-quality metagenome-assembled genomes (HQ-MAGs-based) (B) were used for the RF model, and classifier performance was measured by receiver operating characteristic (ROC) curves and area under the ROC curve (AUC) value.

(legend continued on next page)

(C–F) *Microbial pathway analysis.* Enumeration of the metabolic MetaCyc pathways distinct or shared between SIG1 and/or SIG2 pools of bacteria in the whole cohort of 499 patients with non-small cell lung cancer (NSCLC) are shown in the Venn diagram and Table S3 (C). Beta-diversity (D). Partial least square ordination plot of fecal microbiota MetaCyc pathways in the whole cohort of 499 NSCLC patients treated with ICIs and categorized with TOPOSCORE (black: SIG1+, green: SIG2+). ANOSIM metric defines the separation of the groups; *p* value defines the significance of group separation after 999 permutations of the samples (D). Partial least square discriminant analysis (PLS-DA) and the subsequent variable importance plot (VIP) as a supervised analysis to identify the most discriminant stool MetaCyc microbial pathways for SIG1+ and SIG2+ patients. Mann-Whitney U test *p* values (*$p < 0.05$, **$p < 0.01$, ***$p < 0.001$) are indicated (E). Clustermap of the 499 patients with NSCLC (colored by SIG1+ or SIG2+) forming two clusters following pathway abundances specifically enriched for SIG1 or SIG2 MGSs (F).

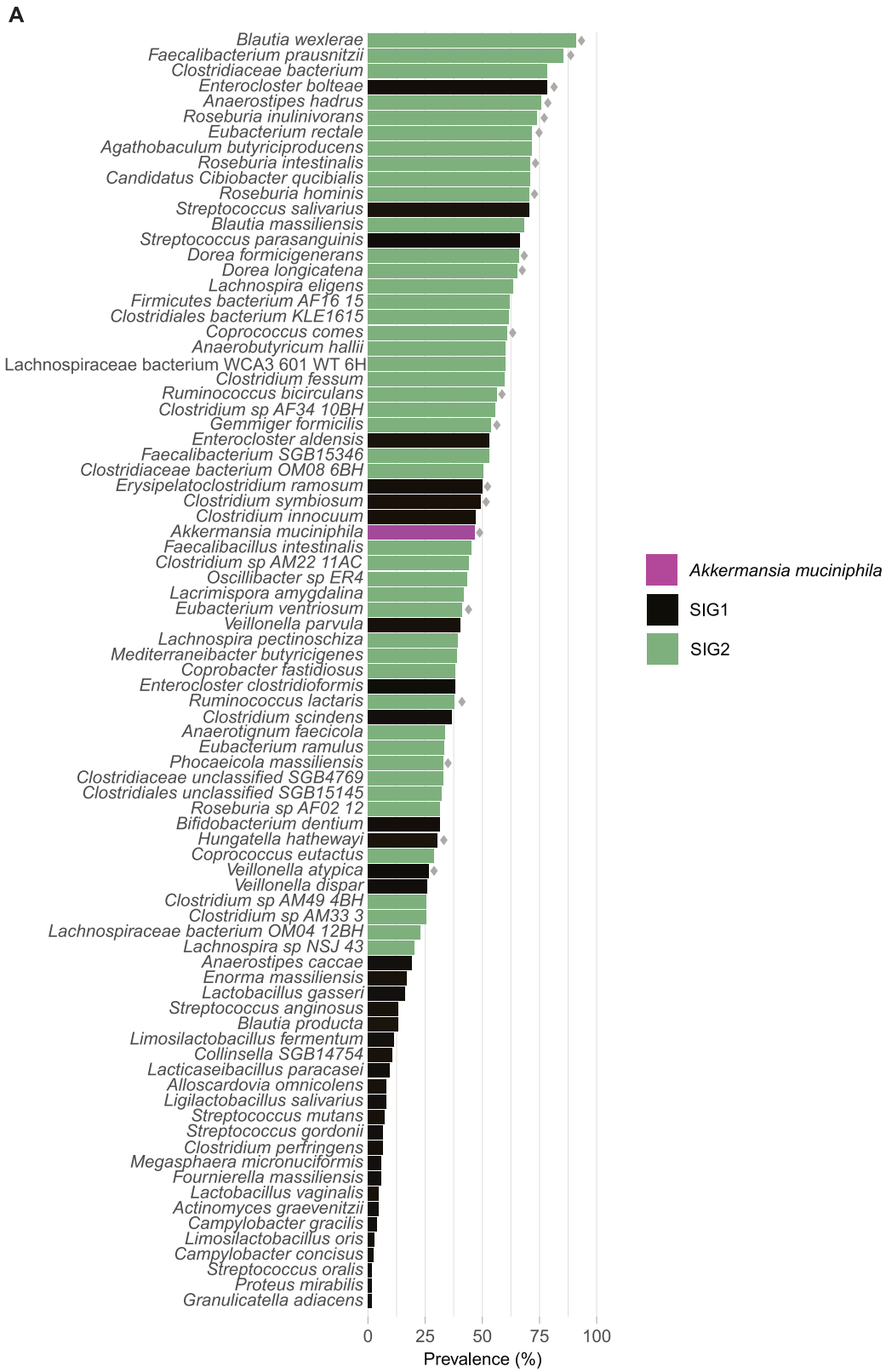

Figure S7. Prevalence of metagenomics species belonging to SIG1 and SIG2

Prevalence of each MGS belonging to SIG1 and SIG2, including the 21 species used in the qPCR-TOPOSCORE (gray diamonds on the right side of bars) in 393 patients with non-small cell lung cancer (NSCLC).

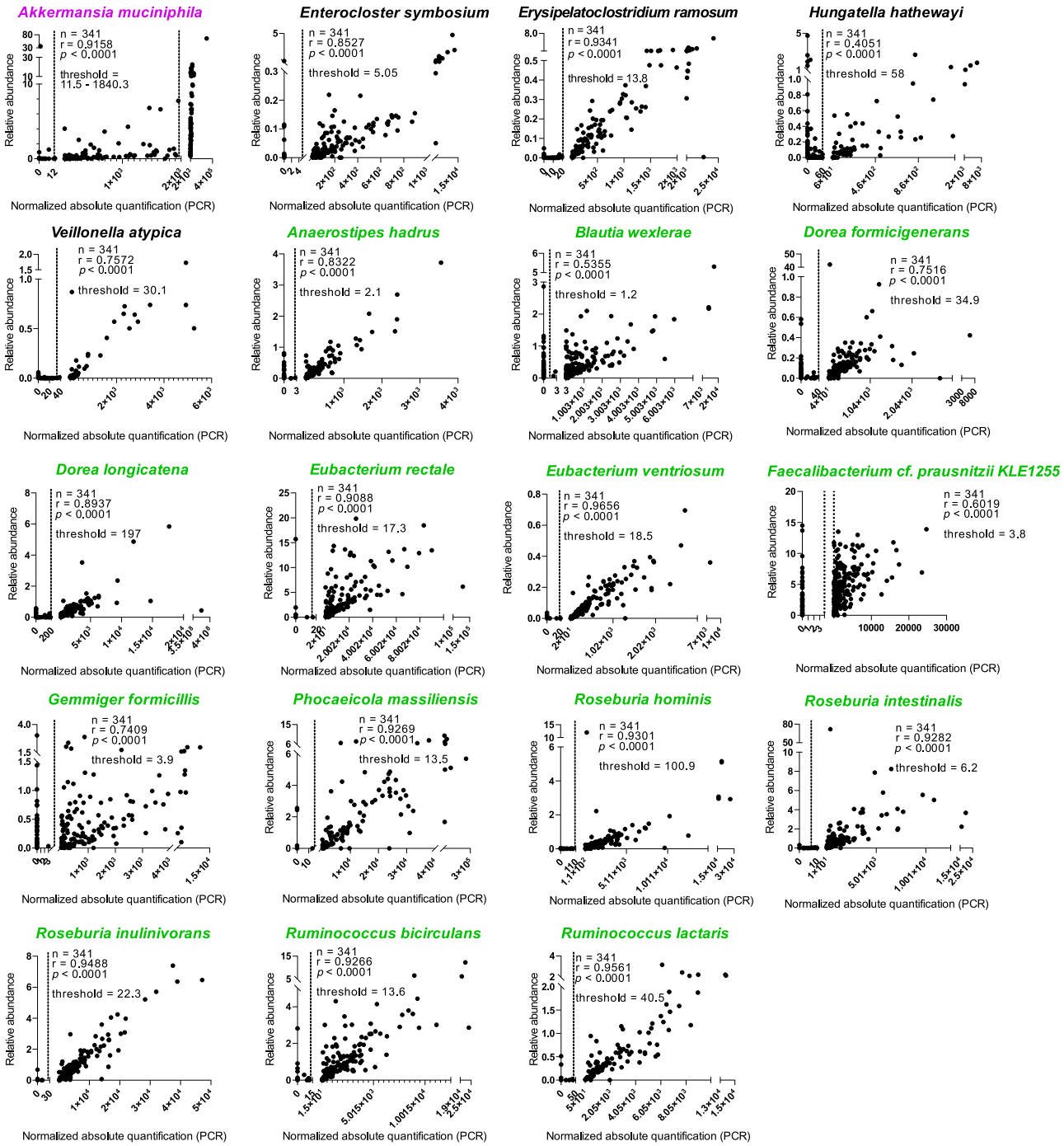

Figure S8. Spearman correlations for microbial abundance between shotgun metagenomics-based sequencing and qPCR

Spearman correlation indices between the two detection methods for each of the 19 bacteria (the two others being presented in Figure 5A) belonging to the TOPOSCORE with their detection thresholds (annotated in Table S6 and dotted line). Normalized values of the qPCR quantification and relative abundances in MG for each bacterium were correlated, the rho and *p* values being annotated for each bacterium. Each dot represents one fecal DNA sample. Each graph depicts the result of one bacterial detection. Of note, we selected the very prevalent (>90%) *Faecalibacterium cf. prausnitzii* KLE1255 corresponding to SGB15342 in MetaPhlAn4 for the qPCR determination of *F. prausnitzii*.